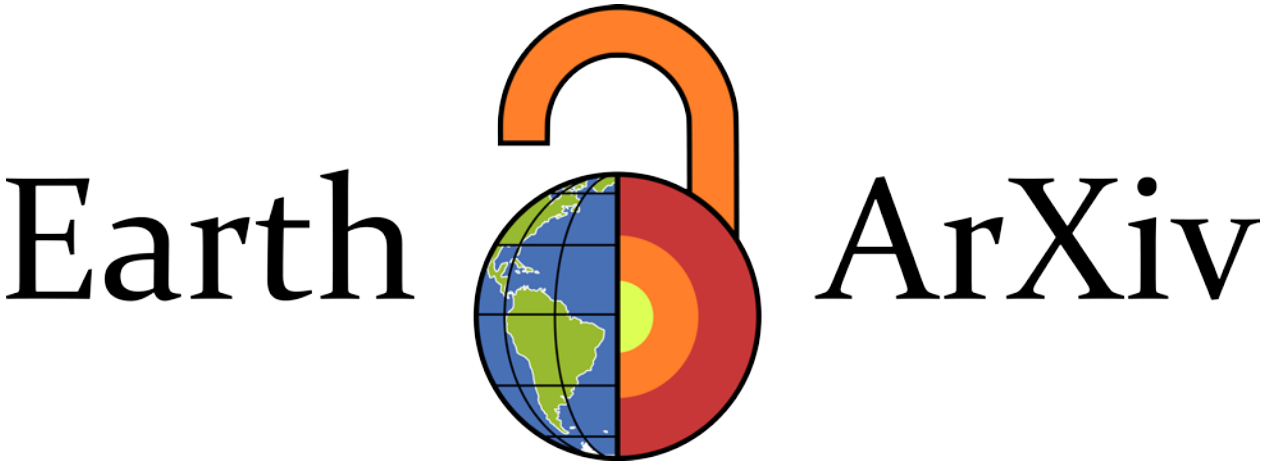

This is a non-peer-reviewed preprint submitted to EarthArXiv.

Harmonized global to regional gridded methane inventories in a discrete global grid framework

Mingke Erin Li[1], Mozhou Gao[2], Steve H.L. Liang[1,2]

[1]Department of Geomatics Engineering, Schulich School of Engineering, University of Calgary, Calgary, Canada
[2]SensorUp Inc., Calgary, Canada

Correspondence to: Mingke Erin Li (mingke.li@ucalgary.ca)

Abstract. Existing gridded methane emission inventories vary widely in resolution, sector schemes, formats, and units, hindering cross-comparison, integration with measurements, and use in emerging analytical frameworks, particularly because latitude-longitude grids have non-uniform cell areas that bias comparison and aggregation. Here, we present a harmonized methane emissions dataset that standardizes 13 heterogeneous gridded inventories across global, continental, national, and regional scales. National datasets include the United States, Canada, Mexico, India, Australia, China, and Switzerland, with emphasis on energy-related emissions from coal mining and oil and gas activities. All inventories were converted into the rearranged Hierarchical Equal Area isoLatitude Pixelization (rHEALPix) Discrete Global Grid System (DGGS) at resolution levels aligned with native spatial scales. Spatial structure, sector classification, and reporting units were standardized, and quantitative validation confirmed high consistency before and after conversion. The resulting dataset offers an equal-area, hierarchical, machine-readable framework enabling consistent comparison and aggregation across sectors, countries, years, and resolutions. The harmonized structure supports applications from atmospheric inversions and hotspot detection to benchmarking, mitigation planning, and AI-ready spatial analysis and model integration.

Background & Summary

Methane is a potent, short-lived greenhouse gas whose mitigation can yield rapid temperature benefits within decades. Its high global warming potential over 20 years and its roughly decade-long atmospheric lifetime make it a prime target for near-term climate risk reduction. Anthropogenic methane originates from diverse human activities, including food production (enteric fermentation, manure, and rice), and energy production (oil, gas, and coal), as well as waste management processes (landfills and wastewater) [1]. Among these, the energy sector is a major contributor, with emissions from fossil fuel production, including petroleum, natural gas, and coal, estimated to account for about 32-34% of global anthropogenic methane [1]. Because many of these emissions originate from controllable processes, mitigation is economically facilitated, with approaches such as leak detection and repair and vent gas capture both technically mature and cost-effective. This makes the energy sector a practical and high-impact focus for methane reduction efforts.

Gridded methane emission inventories (also known as priors) have become core infrastructure for research and decision support. They provide spatially resolved priors for atmospheric inversions, help separate sectoral contributions, and allow comparisons between model outputs and observations. Regional atmospheric inversions in western Canada revealed discrepancies relative to widely used priors [2], satellite-driven analyses in the Permian Basin used gridded priors to contextualize detected variability [3,4], and North American assessments have compared national and continental products to evaluate consistency at multiple scales [4-6]. Beyond inverse modeling, spatially explicit inventories support local and regional assessments, alignment with measurement campaigns, and practical mitigation planning, e.g., reconciling oil-and-gas estimates with site-level measurements [7] or using gridded baselines to detect and simulate short-duration high-emission events [8].

However, spatially synthesizing information across multiple inventories remains challenging. Products differ in their native coordinate reference system (CRS), spatial resolution, file format and structure, sector schemes, and reporting units. Even when each product is internally consistent, these differences complicate like-for-like comparisons, aggregations, and integrations with measurements or models. Furthermore, most gridded inventories are provided on latitude-longitude graticules, where cell areas vary with latitude. This non-uniformity can distort visual interpretation and complicate intensity calculations, particularly at higher latitudes. While some datasets provide per-cell area to aid normalization, comparisons across regions and scales remain non-trivial. In practice, these differences require custom data processing for each analysis, making it difficult to scale, reproduce, or combine results across multiple inventories.

To address these issues, we adopt a Discrete Global Grid System (DGGS) as the standard spatial platform for harmonization. DGGS partition the earth's surface into a globally exhaustive, equal-area, and hierarchically refinable set of cells, each with an identifier that persists across analyses and time [9]. This combination of equal area, hierarchy, and unique indices enables like-for-like comparisons across latitudes, clean aggregation or disaggregation between resolutions, and reliable table-style joins among diverse geospatial datasets [10,11]. Specifically for methane applications, DGGS cells can host gridded fields and point observations, enabling unbiased binning of measurements and inventories into a standard equal-area fabric. DGGS has already proven useful as a data fabric for heterogeneous environmental and socio-economic data, including multi-source maritime risk modeling [12], climate-informed flood mapping with machine learning [13], scalable and interoperable land-use mapping [14], spatial prediction of social phenomena using neural networks [15,16], and the creation of machine-learning-ready spatial databases with thousands of variables at multiple granularities [17].

In this study, we adopted the rearranged Hierarchical Equal Area isoLatitude Pixelization (rHEALPix) DGGS to harmonize 13 open-access, heterogeneous gridded methane emission inventories at global to regional scales. This DGGS-powered approach provides an equal-area, iso-latitude, hierarchically nested tessellation with consistent cell indexing, enabling alignment across spatial resolutions while preserving emission mass for global-to-regional analyses. By converting diverse native grids into the standardized rHEALPix cells, we align the spatial reference (“where” emissions occur), semantic classification (“what” the primary emission sources are, mapped to a consistent sector scheme), and quantitative values (“how much,” unified to a standard mass-per-time unit), resulting in a spatially and semantically coherent dataset optimized for analysis and reuse. The dataset conversion includes three primary steps: (1) we converted heterogeneous source data to a

common raster format with the same CRS; (2) we performed area-weighted intersection to redistribute the raster to the rHEALPix DGGS framework; and (3) we standardized the values to ensure consistency in reporting units and sector schemes across inventories. The objectives of this study are to integrate existing inventories into a unified equal-area DGGS framework, document reproducible harmonization workflows that preserve mass, and facilitate integration with atmospheric models and data assimilation systems. This effort does not re-estimate emissions but focuses on making existing information more comparable, queryable, and actionable. All related data descriptions and data sources can be found in the references and Supplementary Information.

Methods

Input Source Gridded Inventories

This study includes 13 open-source, bottom-up gridded methane inventories developed since 2010 and made publicly accessible through peer-reviewed publications or official repositories. The selected datasets span global, continental (Europe), national (United States, Canada, Mexico, China, Switzerland, India, and Australia), and high-resolution subnational (New York State) inventories. Particular emphasis is placed on energy-related methane emissions, including coal mining and oil and gas systems, given their dominant role in anthropogenic methane budgets and their high relevance for climate mitigation. For datasets available in multiple versions, the most recent release was used in this study, except for the Global Fuel Exploitation Inventory (GFEI), for which three distinct versions corresponding to different reporting years (2016, 2019, and 2020) were included. Table 1 lists spatial coverage, CRS, spatial resolution, temporal coverage, file formats, sector classification schemes, and reporting units. Further details on individual datasets are provided in the Supplementary Information.

These inventories differ substantially in their original formats, CRS, sectoral classification schemes, spatial resolutions, and reporting units. For example, Emissions Database for Global Atmospheric Research (EDGAR) v8.0 Greenhouse Gas Emissions and GFEI provide global grids at 0.1° resolution in NetCDF format under the Geographic Coordinate System WGS84 [18-21]. Several national gridded inventory products adopt the same convention, including the U.S. Anthropogenic Methane Emissions (2012-2018), Canada Anthropogenic Methane Emissions in 2018, and Mexico Anthropogenic Methane Emissions in 2015 [6,22,23]. However, some of the other national datasets follow different approaches, such as China's CHN-CH_4 product at about 10 km resolution in the Krasovsky 1940 Albers projection in GeoTIFF format [24], and Switzerland Greenhouse Gas Inventory at 500 m resolution in CH1903/LV03 with NetCDF format [25]. The Copernicus Atmosphere Monitoring Service Regional (CAMS-REG) emissions inventory provides European coverage at 0.05° × 0.1° resolution on a WGS 84 latitude-longitude grid, distributed as NetCDF or CSV files [26]. The Gridded New York State Methane Emissions Inventory dataset is at 100 m resolution in UTM Zone 18N with NetCDF format [27]. As shown in Table 1, category codes also vary across inventories. Some datasets report emissions directly using Intergovernmental Panel on Climate Change (IPCC) 2006 or 1996 codes, others follow the Common Reporting Tables (CRT), and some lack explicit coding schemes. The CAMS-REG v8.1 Emissions Inventory for Europe adopts the 14-group Gridded Nomenclature for Reporting (GNFR) sector classification, which

is consistent with the reporting conventions used in European air-pollutant inventories [26]. Units span molecules cm^{-2} s^{-1}, kg h^{-1}, Mg km^{-2} a^{-1}, etc., reflecting the heterogeneity in original reporting systems. The CAMS-REG inventory reports emissions in kg m^{-2} s^{-1} or Tg, and in this study, the data were provided in Tg units.

Despite these differences, the inventories share a common methodological foundation. Each is a bottom-up product, typically constructed from national inventory reports submitted to the United Nations Framework Convention on Climate Change (UNFCCC), complemented with sector-specific activity data and emission factors derived from IPCC guidelines or country-specific studies. Spatial allocation to grids is generally achieved using proxy data, including facility locations (e.g., oil and gas wells, coal mines, landfills), infrastructure databases (e.g., pipelines, refineries, wastewater plants), and other geospatial layers such as population, land use, livestock distributions, and satellite products.

Table 1. Summary of source gridded methane emission inventories included in this study.

Dataset	Spatial coverage	CRS	Resolution	Temporal coverage	File format	Category code scheme	Reporting unit	Reference
EDGAR v8.0[1]	Global	Geographic Coordinate System WGS 84	0.1 × 0.1°	1970-2022	NetCDF	IPCC 2006 and IPCC 1996	metric ton a^{-1}	Crippa, et al. [21]
GFEI[2]	Global	Geographic Coordinate System WGS 84	0.1 × 0.1°	2016(v1) 2019(v2) 2020(v3)	NetCDF	IPCC 2006	Mg a^{-1} km^{-2}	Scarpelli, et al. [18],Scarpelli, et al. [19],Scarpelli, et al. [20]
CAMS-REG v8.1[3]	Europe	Geographic Coordinate System WGS 84	0.05 × 0.1°	2005-2022	NetCDF or CSV	GNFR	kg m^{-2} s^{-1} or Tg	Omara, et al. [28]
U.S. Anthropogenic Methane Emissions[4]	Contiguous United States	Geographic Coordinate System WGS 84	0.1 × 0.1°	2012-2018	NetCDF	CRT	molecules CH_4 cm^{-2} s^{-1}	Maasakkers, et al. [22]
Canada Anthropogenic Methane Emissions	Canada	Geographic Coordinate System WGS 84	0.1 × 0.1°	2018	NetCDF	CRT	Mg a^{-1} km^{-2}	Scarpelli, et al. [6]
Mexico Anthropogenic Methane Emissions	Mexico	Geographic Coordinate System WGS 84	0.1 × 0.1°	2015	NetCDF	IPCC 2006	Mg a^{-1} km^{-2}	Scarpelli, et al. [23]
China Anthropogenic Methane Emissions	China	Krasovsky 1940 Albers projection	~10 × 10 km	1990-2020	GeoTIFF	-	Mg a^{-1} km^{-2}	Guo, et al. [24]
Switzerland Greenhouse Gas Inventory	Switzerland	Swiss CH1903/ LV03	500 × 500m	2011	NetCDF	-	g m^{-2} a^{-1}	Hiller, et al. [25]
U.S. Oil and Gas Methane Emissions	Contiguous United States	Geographic Coordinate System WGS 84	0.1 × 0.1°	2021	NetCDF	-	kg h^{-1}	Omara, et al. [28]
CMS Datasets on Methane Flux for Oil and Gas Systems[5]	Canada Mexico	Geographic Coordinate System WGS 84	0.1 × 0.1°	2013 2010	NetCDF	-	molecules CH_4 cm^{-2} s^{-1}	Sheng, et al. [29]
China Coal Mine Methane Emissions	China	Geographic Coordinate System WGS 84	0.25 × 0.25°	2011	NetCDF	-	Mg a^{-1} km^{-2}	Sheng, et al. [30]
India and Australia Coal Mine Methane Emissions	India and Australia	Geographic Coordinate System WGS 84	0.1 × 0.1°	2018	CSV	-	metric ton a^{-1}	Sadavarte, et al. [31]
Gridded New York State Methane Emissions[6]	New York State	UTM Zone 18N projection	100 × 100m	2020	NetCDF	IPCC 1996	kg m^{-2} s^{-1}	Loman, et al. [27]

[1] Emissions Database for Global Atmospheric Research (EDGAR). EDGAR v8.0 provides estimates of emissions from the three leading greenhouse gases (CO2, CH4, and N2O) and fluorinated gases, per sector and country, and we only include CH_4 emissions.
[2] Global Fuel Exploitation Inventory (GFEI). Three publicly available versions correspond to 2016, 2019, and 2020. According to the data description, additional emission grids for 2010-2019 are available upon request, but only the three accessible years are included here.

[3] Copernicus Atmosphere Monitoring Service Regional (CAMS-REG) v8.1 Emissions Inventory for Europe. It includes CH_4 alongside the major air pollutants NO_x, SO_2, CO, NH_3, NMVOC, PM_{10}, and $PM_{2.5}$ with full sectoral detail.
[4] Monthly emission scaling factors are available for the Gridded Annual U.S. Anthropogenic Methane Emissions (2012-2018) covering 26 source categories (Gridded GHGI). An additional 'Express Extension' provides gridded annual emissions for 2012-2020 with 27 source categories. In this dataset, we include only the Gridded GHGI and exclude the Express Extension.
[5] Carbon Monitoring System (CMS) data sets on Methane Flux for Canadian and Mexican Oil and Gas Systems. The dataset is available for Canada in 2013 and Mexico in 2010.
[6] Monthly scaling factors and weekday scaling factors are also available in the source datasets.

rHEALPix DGGS Framework

The rHEALPix DGGS is a geospatial extension of the HEALPix system, initially designed for astronomy and later adapted for Earth science applications [32,33]. Its defining features include equal-area cells, hierarchical tessellation, and iso-latitude cell distribution, which together enable consistent spatial representation across the globe [33]. Unlike traditional graticule-based grids, rHEALPix avoids latitude-dependent distortions in cell size, ensuring that emission intensities are directly comparable across regions. Its hierarchical indexing supports seamless aggregation from fine to coarse resolutions by querying cell indices with a common prefix, while its congruent and orientation-preserving tessellation reduces computational complexity during multi-resolution analysis. These properties make rHEALPix particularly suited for harmonizing heterogeneous methane emission inventories, providing a uniform, scalable framework for cross-scale analysis, hotspot detection, and integration with atmospheric models (Fig. 1). The advantages of using the rHEALPix DGGS for global gridded methane inventories have been discussed in detail in our previous work [34].

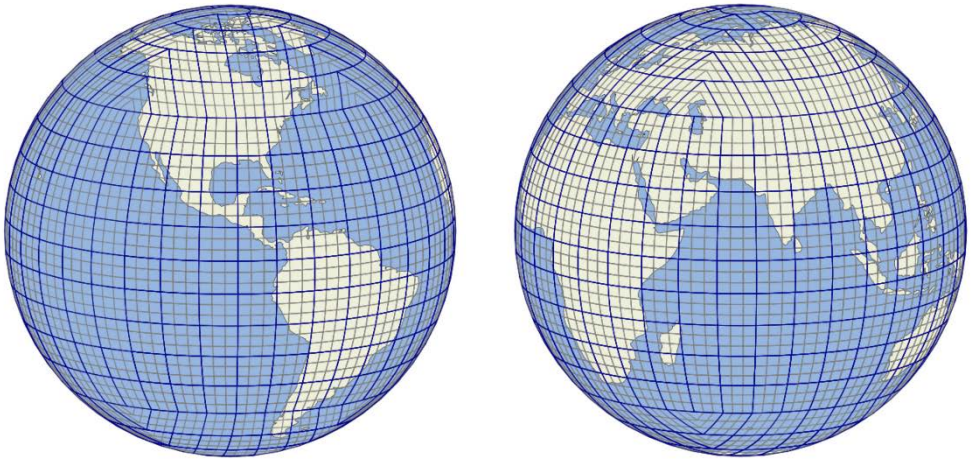

Fig. 1 Overview of the rHEALPix DGGS at resolution levels 2 and 3.

We used the DGGAL library for rHEALPix grid generation and indexing with a refinement ratio of nine [35]. The grid creation process was designed to ensure coverage of both terrestrial and offshore sources. First, country geometries from the Database of Global Administrative Areas (GADM) were used to generate rHEALPix cells to define land-based grids [36]. Second, offshore

oil and gas facilities were extracted from the Oil and Gas Infrastructure Mapping (OGIM) database, including tank batteries, petroleum terminals, compressor stations, injection or disposal sites, and other offshore facilities [37]. The locations of these facilities were buffered to represent their operational footprints, and the resulting buffered geometries were used to generate rHEALPix cells. The land-based and offshore grids were then combined, duplicates removed, and International Organization for Standardization (ISO) country codes assigned for standardized referencing.

Resolution levels of rHEALPix DGGS were chosen to align with the native resolution of each inventory. Table 2 lists the specific characteristics of rHEALPix DGGS at different resolutions, including the average ellipsoidal cell size and the planar cell width. For the Gridded New York State Methane Emissions Inventory dataset (100 × 100 m, about 0.01 km²), we selected rHEALPix level 10 (about 0.02 km²). For the Switzerland Greenhouse Gas Inventory (500 × 500 m, 0.25 km²), level 9 was used (about 0.22 km²). For CAMS-REG at 0.05 × 0.1° resolution, we adopted rHEALPix level 7 (about 17.8 km²). For other global and national inventories with native resolution of 0.1° (about 10 × 10 km), we adopted level 6 (about 160 km²). An exception was made for the China coal mine dataset at 0.25° resolution (about 25 × 25 km), although coarser than most, it was mapped at level 6 rather than level 5 (about 1441 km²) to avoid over-smoothing. All grids were generated programmatically using the DGGAL API, ensuring consistency across datasets and facilitating reproducible integration of diverse inventories into the DGGS framework [35].

Table 2. Summary of the rHEALPix DGGS cell dimensions across resolutions.

Resolution level	Average cell width (m, planar)	Average cell area (m^2, ellipsoidal)
0	1.00×10^7	8.51×10^{13}
1	3.34×10^6	9.46×10^{12}
2	1.11×10^6	1.05×10^{12}
3	3.71×10^5	1.17×10^{11}
4	1.24×10^5	1.30×10^{10}
5	4.12×10^4	1.44×10^9
6	1.37×10^4	1.60×10^8
7	4.58×10^3	1.78×10^7
8	1.53×10^3	1.98×10^6
9	509	2.20×10^5
10	170	24408
11	56.5	2712
12	18.8	301
13	6.28	33.5
14	2.09	3.72
15	0.698	0.413

Spatial Processing

The source inventories used in this study were published in different formats, including NetCDF, CSV, and GeoTIFF, each requiring pre-processing before DGGS conversion. NetCDF files (e.g., EDGAR, GFEI, CAMS-REG, and most of the national gridded inventories) typically contain gridded arrays with latitude-longitude or projected coordinates, time dimensions, and sector-specific variables [6,19-23,26]. CSV files (e.g., India and Australia Coal Mine Methane Emissions Inventories in 2018) provide point-based grids with explicit latitude, longitude, and emission values [31]. The China Anthropogenic Methane

Emissions Inventories are distributed as annual GeoTIFF rasters [24]. For consistency, all inputs were first converted to intermediate raster representations, ensuring one raster per reporting category. Pixel centers were used to define raster alignment, with coordinate transforms shifted by half a pixel to match native grid definitions. When necessary, latitude arrays were reversed to match top-to-bottom raster conventions.

Differences in CRS were harmonized by reprojecting all datasets to the Geographic Coordinate System WGS84 before raster conversion, when necessary (e.g., the Switzerland Greenhouse Gas Inventory in CH1903/LV03 and the Gridded New York State Methane Emissions Inventory in UTM 18N). For projected datasets, pixel areas were calculated directly from affine transforms to account for variable cell sizes. For geographic datasets (EPSG:4326), pixel areas were derived from spherical geometry or, when available, read from the area attributes in the source datasets.

Following rasterization, emissions were redistributed to the rHEALPix DGGS framework using an area-weighted approach. Each raster pixel was intersected with overlapping DGGS cells, and emissions were proportionally allocated based on the area of overlap. The raster-first approach was adopted for computational efficiency, meaning that non-zero raster pixels were first filtered and their overlapping DGGS cells were identified. Afterward, the contribution of each pixel to the intersecting DGGS cells was calculated based on the area of overlap. This procedure reduced unnecessary geometric operations by limiting calculations to relevant grid cells. The Python package 'uraster' was developed to accomplish this task[38]. To ensure mass conservation, a scaling factor was applied to preserve the total emissions before and after DGGS conversion. For continental, national, and regional datasets, the applied scaling factors were very close to 1, confirming that redistribution introduced minimal numerical deviation. For global inventories, scaling factors were calculated separately for each country, category, and year, ensuring that country-level totals were accurately retained.

The implementation was optimized for efficiency through parallel processing, which distributed category- and year-specific calculations across multiple cores. A raster-first approach minimized geometric overhead, while spatial indexing and bounding box pre-filtering limited intersection checks to relevant pixels and DGGS cells. These strategies reduced computation time and memory demands, enabling consistent processing of both extensive global inventories and fine-scale regional datasets. Fig. 2 illustrates the workflow from the original inventories to the DGGS outputs. All computations in this study were performed on the Advanced Research Computing (ARC) high-performance cluster at the University of Calgary.

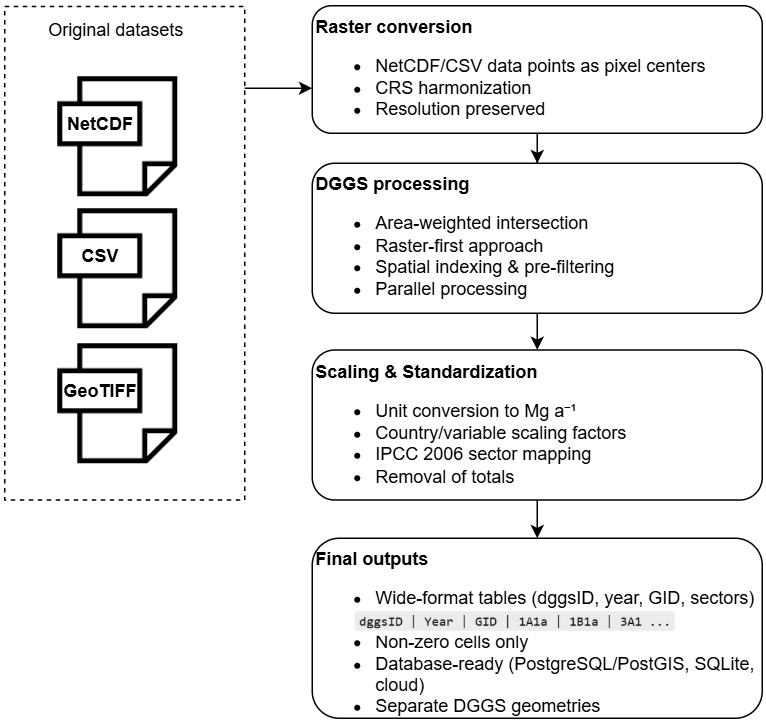

Fig. 2 Workflow of converting original gridded methane inventories to DGGS.

Unit Standardization

Source inventories report methane in heterogeneous units, such as fluxes and areal intensities. For comparability in an equal-area DGGS, all variables were converted to megagrams per year (Mg a^{-1}) at the cell level. When inputs were reported as rates per area, we first computed per-pixel totals by multiplying by the pixel area in the native CRS, then mapped to DGGS and conserved mass via the scaling step (Section 3.2). Below are the unit transformations used throughout.

For inventories reported in Mg a^{-1} km^{-2} e.g. GFEI; [19], values were first converted to per-m^2 fluxes by applying a factor of 10^{-6}, and then multiplied by the pixel area in square meters to obtain per-pixel totals (Eq. 1):

$$E_{Mg\ a^{-1}} = V_{Mg\ a^{-1}\ km^{-2}} \times 10^{-6} \times A_{pixel,m^2} \quad (1)$$

For fluxes reported in kg m^{-2} s^{-1} e.g., Gridded New York State Methane Emissions Inventory; [27], the calculation involved multiplying by pixel area and the number of seconds per year, followed by conversion from kilograms to megagrams (Eq. 2):

$$E_{Mg\ a^{-1}} = V_{kg\ m^{-2}\ s^{-1}} \times A_{pixel,m^2} \times 31{,}536{,}000 \times 10^{-3} \quad (2)$$

For emission rates in kg h^{-1} e.g., U.S. Oil and Gas Methane Emissions; [28], a similar approach was applied by scaling by the total hours per year and converting from kilograms to megagrams (Eq. 3):

$$E_{Mg\ a^{-1}} = V_{kg\ h^{-1}} \times 8{,}760 \times 10^{-3} \quad (3)$$

The national inventories reporting emissions in g m^{-2} a^{-1} e.g., Switzerland Greenhouse Gas Inventory; [25] were converted by multiplying by pixel area and scaling from grams to megagrams (Eq. 4):

$$E_{Mg\ a^{-1}} = V_{g\ m^{-2}\ a^{-1}} \times A_{pixel,m^2} \times 10^{-6} \quad (4)$$

Finally, for datasets expressed as molecules CH_4 cm^{-2} s^{-1} e.g., U.S. Anthropogenic Methane Emissions; [22], a molecular-to-mass conversion was required. Emissions were first multiplied by pixel area (cm^2) and seconds per year, then divided by Avogadro's number to obtain moles of methane. This was converted to grams using the molecular weight of CH_4 (16.04 g mol^{-1}), and finally to megagrams (Eq. 5):

$$E_{Mg\ a^{-1}} = (V_{molec\ cm^{-2}\ s^{-1}} \times A_{pixel,cm^2} \times 31{,}536{,}000 \div N_A) \times M_{CH_4} \times 10^{-6} \quad (5)$$

where $N_A = 6.022 \times 10^{23} mol^{-1}$ is Avogadro's number and $M_{CH_4} = 16.04 g\ mol^{-1}$ is the molecular weight of methane.

For datasets already in metric tons per year, values were carried through unchanged. By expressing every variable as Mg a^{-1} per DGGS cell on an equal-area grid, the resulting fields are globally comparable without latitude-dependent area bias and can be directly summed across cells, sectors, or jurisdictions.

Sector Harmonization

To ensure comparability across heterogeneous methane inventories, all source datasets were harmonized to the IPCC 2006 sector classification. The IPCC 2006 Guidelines for National Greenhouse Gas Inventories define a hierarchical code structure, where top-level categories (e.g., 1 Energy, 2 Industrial Processes and Product Use, 3 Agriculture, Forestry, and Other Land Use, and 4 Waste) are subdivided into finer classes (e.g., 1.A Fuel Combustion Activities, 1.B Fugitive Emissions, 1.C Carbon dioxide Transport and Storage). This hierarchical structure supports aggregation at different levels of detail while maintaining consistency with official reporting standards. It should be noted that the codes cannot always be safely grouped by simple prefix matching, since some subcategories (e.g., 1B2ai and 1B2aii) share prefixes but represent parallel classes at the same hierarchical level due to the use of Roman numerals in the coding system.

Several inventories already provided IPCC 2006 codes for each variable, which were adopted directly. When an original variable represented multiple IPCC 2006 sector codes, for example, "emis_ch4_1A3a,c,d" in the Mexico Anthropogenic Methane Emissions dataset [23], the corresponding codes were merged into a single combined label using a plus sign, resulting in "1A3a+1A3c+1A3d" in this case. Others reported emissions under GNFR codes, CRT codes, or IPCC 1996 codes, where crosswalks were applied to align the reported sectors with their corresponding IPCC 2006 categories [39]. For variables that included both a coarse code level and a descriptive label, the variable was assigned either the original coarse code or a finer-level IPCC 2006 category code, whichever was more appropriate based on the sector definition. For example, the variable "3A (enteric fermentation) - Buffalo" in the Canada Anthropogenic Methane Emissions inventory [6] uses the coarse CRT code "3A," but was reassigned to 3A1b following the IPCC 2006 Reporting Guidance [40], where the subcategory explicitly represents emissions from enteric fermentation of buffalo. During processing and in the final output, a single value is retained for each

unique IPCC 2006 category code. This is achieved by aggregating variables that share the same code and summing their emission values. For datasets containing only text-based variable names without a code scheme, each variable was assigned the closest IPCC 2006 category code, based on careful examination of the original publications and sector definitions. This process ensured a consistent, hierarchical classification system across all inventories. An exception was the Swiss Greenhouse Gas Inventory, which includes natural and semi-natural methane fluxes such as lakes, wetlands, wild animals, and forest soils. Because these sources are not part of the IPCC's anthropogenic reporting structure, they were retained under their original text labels. Finally, to avoid double-counting, “total” categories present in some inventories were excluded during processing. This ensured that each variable is uniquely assigned to a single IPCC 2006 category code, with no overlaps across categories in each dataset.

Data Record

The harmonized dataset includes 13 methane inventories spanning various spatial scales and temporal ranges, collectively representing over 4.1 million non-zero rHEALPix DGGS cells. The data were exported in a tabular format optimized for interoperability and analysis efficiency. Each row of data corresponds to a unique combination of an rHEALPix DGGS cell identifier and a calendar year, ensuring one observation per cell-year pair. Columns represent IPCC 2006 emission categories or subcategories. For global inventories, an additional column records the ISO 3166-1 alpha-3 country code to facilitate country-level aggregation. This structure enables direct access to sector-specific emissions while supporting aggregation to higher-level categories via IPCC code prefixes. Nonetheless, the codes cannot always be reliably grouped by simple prefix matching because the coding system uses Roman numerals. The number of retained IPCC 2006 categories per inventory ranges from 1 (for single-sector datasets such as coal-mine methane) to over 50 (for national inventories with detailed source disaggregation), reflecting the sectoral detail available in the original inventory. To ensure consistency, all emissions values are reported in units of Mg a^{-1}. Rows with all-zero sector values were removed to reduce file size and improve performance. Geometries were not embedded within the tables but are provided separately as GeoParquet files that define polygon boundaries for rHEALPix cells at specific resolutions. This design allows attribute tables to be seamlessly integrated into relational databases or analytical workflows while remaining compatible with geospatial visualization tools through joins with the geometry files. The standardized global to regional gridded methane inventories on rHEALPix DGGS are stored in the Zenodo repository: https://doi.org/10.5281/zenodo.17362125.

Data Overview

Table 3 summarizes the spatial and temporal coverage, DGGS resolution level, number of DGGS cells with non-zero values, and number of IPCC 2006 categories of converted methane inventories in the rHEALPix DGGS. Fig. 3 shows the spatial coverage of the 13 methane inventories included in this study after conversion to rHEALPix DGGS. Although 13 inventories

are included in total, 15 individual datasets are displayed on the map because two inventories cover multiple countries, namely the Carbon Monitoring System (CMS) Datasets on Methane Flux for Canadian and Mexican Oil and Gas Systems and the Coal Mine Methane Emissions inventories for India and Australia [29,31]. Most datasets were mapped at DGGS level 6 (about 160 km²), while fine-scale inventories such as CAMS-REG v8.1 Emissions Inventory for Europe (0.05 × 0.1°), the Switzerland Greenhouse Gas Inventory (500 m), and the Gridded New York State dataset (100 m) required higher resolutions of levels 7, 9 and 10, respectively.

Table 3. Summary of converted methane inventories in DGGS, including the spatial and temporal coverage, DGGS resolution level, number of DGGS cells with non-zero values, and number of IPCC 2006 categories.

Data Source[1]	Spatial coverage	Year Range	DGGS Resolution	Number of non-zero DGGS Cells	Number of IPCC 2006 Categories
EDGAR v8.0	Global	1970-2022	6	847790	21
GFEI	Global	2016(v1) 2019(v2) 2020(v3)	6	764949	15
CAMS-REG v8.1	Europe	2005-2022	7	358928	12
U.S. Anthropogenic Methane Emissions[3]	Contiguous United States	2012-2018	6	50874	25
Canada Anthropogenic Methane Emissions	Canada	2018	6	55182	52
Mexico Anthropogenic Methane Emissions	Mexico	2015	6	13030	45
China Anthropogenic Methane Emissions	China	1990-2020	6	59627	8
Switzerland Greenhouse Gas Inventory	Switzerland	2011	9	189148	8
U.S. Oil and Gas Methane Emissions	Contiguous United States	2021	6	27446	1
CMS Datasets on Methane Flux for Oil and Gas Systems[4]	Canada	2013	6	32277	5
	Mexico	2010	6	10486	5
China Coal Mine Methane Emissions	China	2011	6	10680	1
India and Australia Coal Mine Methane Emissions	India	2018	6	150	1
	Australia	2018	6	83	1
Gridded New York State Methane Emissions	New York State	2020	10	2657699	34

[1] Refer to Table 1 for dataset abbreviations.

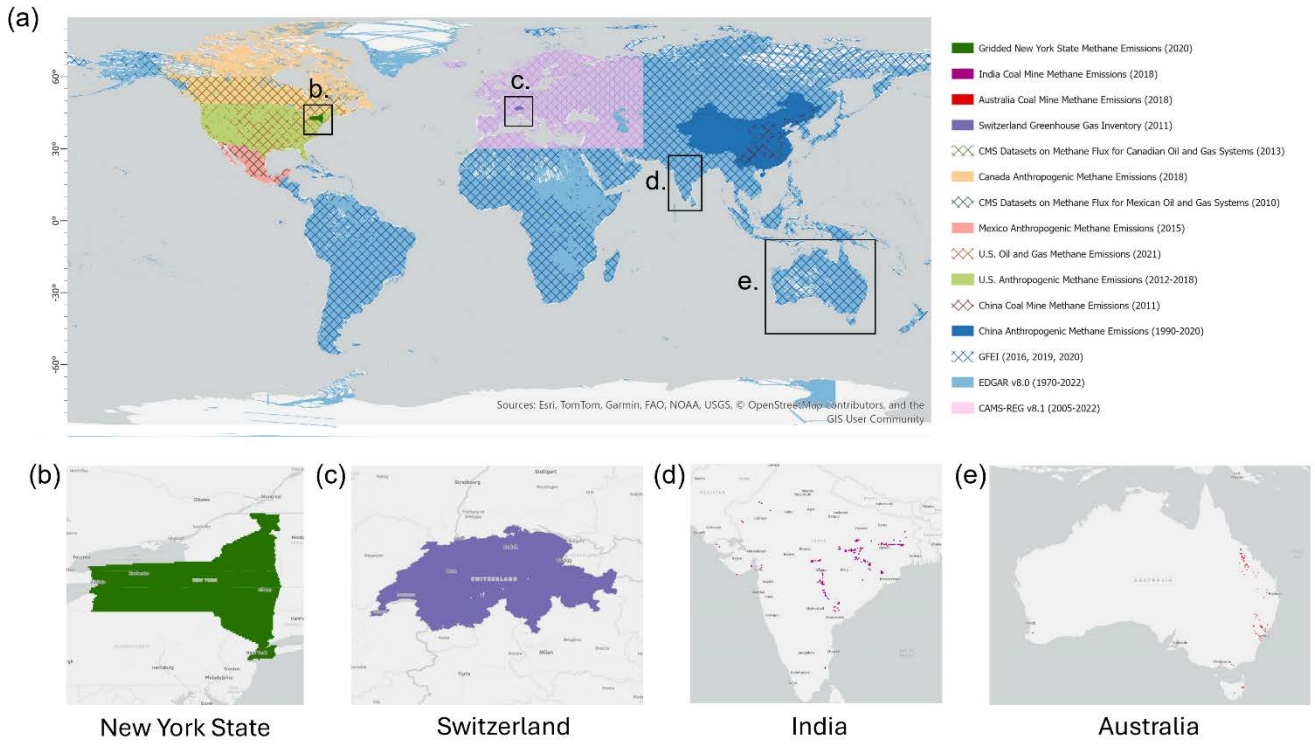

Fig. 3 Spatial coverage of the 13 methane inventories included in this study after conversion to rHEALPix DGGS. (a) Global map showing overlapping extents of global, continental, national, and regional inventories. Crosshatch patterns indicate overlapping datasets with smaller spatial domains. Panels (b-e) provide zoomed-in examples of regional inventories: (b) New York State (2020), (c) Switzerland (2011), (d) India (2018), and (e) Australia (2018).

Technical Validation

Quantitative Validation of DGGS Conversion

Because the DGGS conversion involves a spatial re-aggregation rather than a one-to-one mapping, direct cell-by-cell comparisons between the original and DGGS-based datasets are not meaningful. Instead, evaluation focuses on assessing numerical consistency at the aggregate level before and after conversion to the rHEALPix DGGS for each inventory. Three metrics are used for this purpose: (1) Relative difference is used to quantify year-specific deviations in total in a scale-dependent manner. (2) Normalized root-mean-square error (RMSE) provides a dimensionless measure of the typical discrepancy across the time series, especially for datasets that contain multiple years, such as EDGAR v8.0 and CAMS-REG v8.1. (3) Normalized Mean Bias (MB) is reported to diagnose any systematic increase or decrease introduced by the conversion process.

Table 4 (also see the Supplementary Information) summarizes the relative difference in total emissions before and after conversion for all datasets. For Continental, national and regional datasets, relative differences are negligible, demonstrating

effective conservation of mass during rasterization and cell-to-cell redistribution: Mexico (9.48×10^{-4} %), Switzerland (3.03×10^{-5} %), U.S. Oil and Gas 1.26×10^{-4} %), CMS-Canada (0.03%) and CMS-Mexico (0.01%), China Coal Mine (5.63×10^{-14} %), India/Australia Coal Mine (3.64×10^{-6} % and 7.25×10^{-6} %), and New York State (2.10×10^{-5} %). Canada anthropogenic methane (2018) shows a small 0.25% difference. For the U.S. Anthropogenic Methane Emissions time series, annual relative differences over 2012-2018 range from 0.26% to 0.57% with a mean of 0.43% (Table S3). The CAMS-REG v8.1 Emissions Inventory for Europe and China Anthropogenic Methane Emissions series are effectively identical before and after conversion for all years (Table S2 and S4). Global inventories show slightly higher but still minor relative differences. EDGAR v8.0 ranges from 0.14 to 1.54% across 1970-2022 with an average of 1.03% (Table S1), and GFEI differences are 2.58% (2016 v1), 3.07% (2019 v2), and 2.77% (2020 v3), as shown in Table 4. These modest increases reflect the design choice to apply scaling factors per country, category, and year to preserve country-level totals. When globally re-aggregated after area-weighted mapping to equal-area cells, minor rounding and boundary effects accumulate, resulting in slightly higher discrepancies than for single-country datasets. Table 5 reports the normalized RMSE and MB of annual totals before and after conversion to the DGGS framework for four multi-year datasets. In all cases, both metrics are close to zero, indicating negligible numerical discrepancies associated with the area-weighted spatial re-aggregation. CAMS-REG v8.1 (1.14×10^{-7}) and China Anthropogenic Methane Emissions (6.45×10^{-11}) show values near machine precision, while EDGAR v8.0 and U.S. Anthropogenic Methane Emissions exhibit slightly larger but still small, normalized errors (<1%). These results confirm that the DGGS conversion preserves annual totals without introducing systematic errors.

Table 4. Comparison of total methane emissions before and after conversion to rHEALPix DGGS for all inventories included in this study. For EDGAR v8.0, CAMS-REG v8.1, U.S. Anthropogenic Methane Emissions, and China Anthropogenic Methane Emissions, only selected benchmark years are shown here; the full annual comparisons for EDGAR v8.0 (1970–2022), CAMS-REG v8.1 (2005-2022), U.S. (2012–2018), and China (1990–2020) are provided in the Supplementary Information.

Data Source[1]	Year	Total Emissions before Conversion (Mg a^{-1})[2]	Total Emissions after Conversion (Mg a^{-1})	Relative Difference (%)
EDGAR v8.0	1970	309013762.78	308362819.28	0.21
	1980	342221909.20	338802272.29	1.00
	1990	371245211.61	366800813.02	1.20
	2000	386244031.24	378407739.96	2.03
	2010	449276495.57	439754822.30	2.12
	2020	485252085.38	475908820.84	1.93
GFEI	2016	97224636.28	94719841.73	2.58
	2019	80419238.44	77949246.12	3.07
	2020	73874620.47	71831885.04	2.77
CAMS-REG v8.1	2005	58948955	58948948	-1.18E-05
	2010	56851049	56851037	-2.15E-05
	2015	57048963	57048966	4.66E-06
	2020	59307306	59307311	9.47E-06
U.S. Anthropogenic Methane Emissions	2012	25626259.09	25692238.00	0.26
	2015	25370927.66	25503835.72	0.52
	2018	25225964.39	25368622.74	0.57

Canada Anthropogenic Methane Emissions	2018	3655967.45	3646964.48	0.25
Mexico Anthropogenic Methane Emissions	2015	5076752.83	5076704.68	9.48E-04
China Anthropogenic Methane Emissions	1990	24676397.28	24676397.28	1.27E-10
	2000	28417742.36	28417742.36	7.99E-11
	2010	45339490.63	45339490.62	1.88E-11
	2020	46431934.67	46431934.67	2.32E-10
Switzerland Greenhouse Gas Inventory[3]	2011	162409.70	162409.65	3.03E-05
U.S. Oil and Gas Methane Emissions	2021	15610442.12	15610422.41	1.26E-04
CMS Datasets on Methane Flux for Oil and Gas Systems	2013 (Canada)	2329955.38	2329312.28	0.03
	2010 (Mexico)	1159660.12	1159510.24	0.01
China Coal Mine Methane Emissions	2011	16555455.86	16555455.86	5.63E-14
India and Australia Coal Mine Methane Emissions	2018 (India)	823149.22	823149.25	3.64E-06
	2018 (Australia)	969134.07	969134.00	7.25E-06
Gridded New York State Methane Emissions	2020	690582.43	690582.28	2.10E-05

[1] Refer to Table 1 for dataset abbreviations.
[2] Reported values from the original datasets were standardized to units of Mg a^{-1} for consistency and comparison.
[3] The Switzerland Greenhouse Gas Inventory includes both anthropogenic and natural methane emission sources.

Table 5. Normalized root-mean-square error (RMSE) and normalized mean bias (MB) of annual emission totals before and after conversion to the DGGS framework, for four multi-year datasets.

Data Source[1]	Normalized root-mean-square error (RMSE)	Normalized Mean Bias (MB)
EDGAR v8.0	0.00953527	-0.008561952
CAMS-REG v8.1	1.14E-07	3.44E-08
U.S. Anthropogenic Methane Emissions	0.004358996	0.004208769
China Anthropogenic Methane Emissions	6.45E-11	-2.01E-11

[1] Refer to Table 1 for dataset abbreviations.

Overall, the DGGS conversion process successfully preserves mass at intended aggregation levels and provides a consistent, equal-area representation. All scaling factors were applied deterministically, and the processing code is openly available, ensuring full traceability from original grids to DGGS outputs. These results demonstrate that the harmonization achieves mass balance, internal consistency, and reproducibility, supporting robust use in analytical and modeling applications.

Visualization of Harmonized Emission Patterns

To illustrate how the harmonized products enable like-for-like visualization of energy-sector emissions, we render multiple inventories in identical units (Mg a^{-1} per DGGS cell) on the rHEALPix grid. Although a map projection is used for display, the underlying equal-area tessellation ensures that cell areas remain effectively uniform, and the visual impression of intensity is therefore independent of the chosen projection and directly comparable across panels [10]. Fig. 4 presents global fuel-exploitation emissions for common years (2016, 2019, 2020) from EDGAR v8.0 and GFEI at DGGS level 6 using the same color scale. For EDGAR, fuel exploitation is the sum of the component variables reported for coal, gas, and oil (original categories PRO_COAL, PRO_GAS, and PRO_OIL). The side-by-side maps demonstrate that heterogeneous source variables from distinct global inventories can be standardized and displayed coherently once mapped to the DGGS.

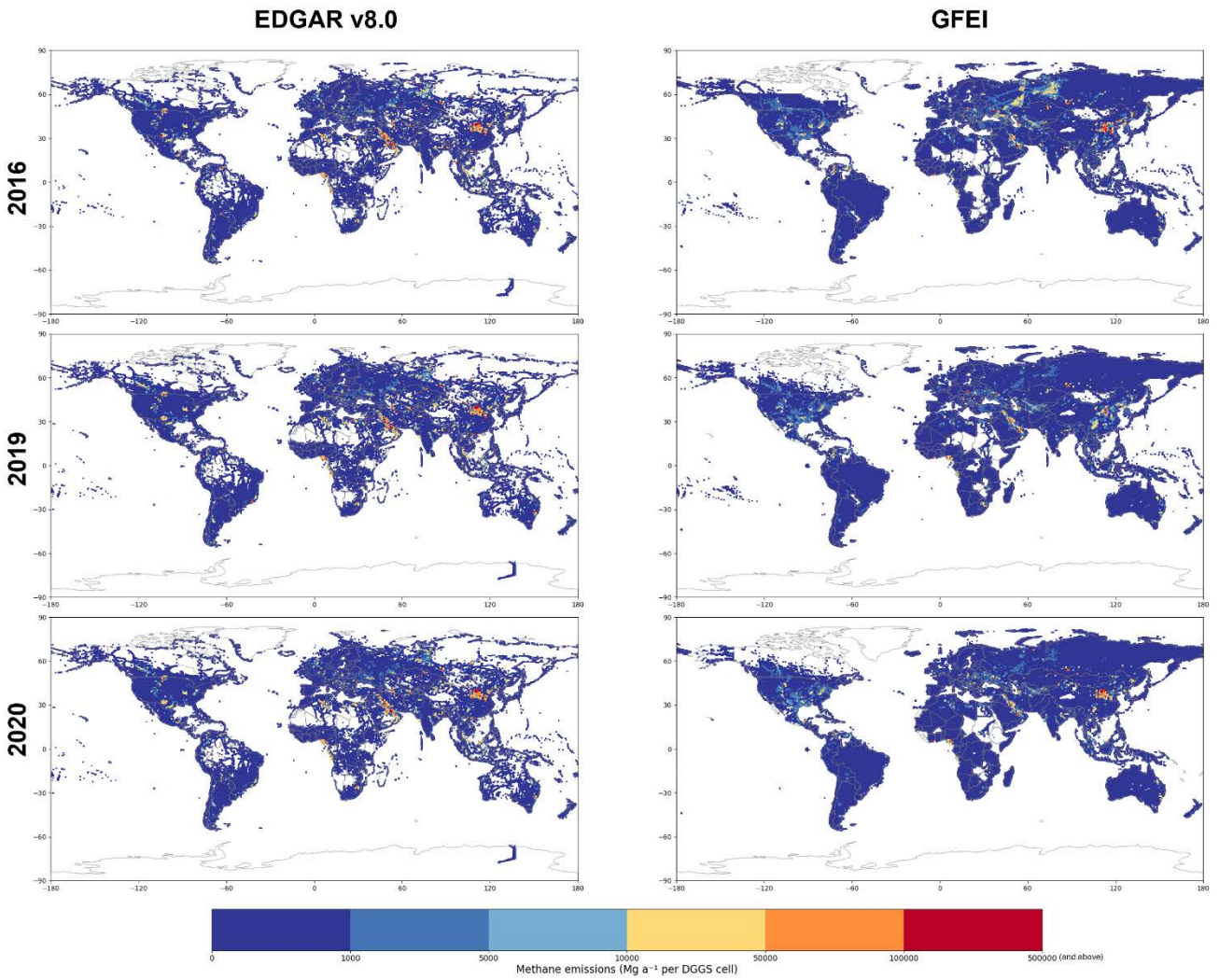

Fig. 4 Methane emissions from fuel exploitation (Mg a^{-1} per DGGS cell) derived from EDGAR v8.0 (left) and GFEI (right) for common reporting years 2016, 2019, and 2020, after conversion to the rHEALPix DGGS at resolution level 6 [18-21].

At the national scale (Fig. 5), single-year products for U.S. oil and gas (2021), China coal mining (2011), and the CMS oil-and-gas datasets for Canada (2013) and Mexico (2010) are shown with identical symbology at level 6 [28-30]. These panels are intended to be illustrative rather than evaluative. Each dataset originates from different methodologies and reporting conventions, while all can be presented with a common legend and equal-area grid, allowing immediate visual comparison of spatial distributions without implying cross-dataset ranking or accuracy assessment. The uniform treatment of units, sector coding, and grid geometry makes differences in spatial structure legible while avoiding artifacts associated with differing native projections or cell sizes.

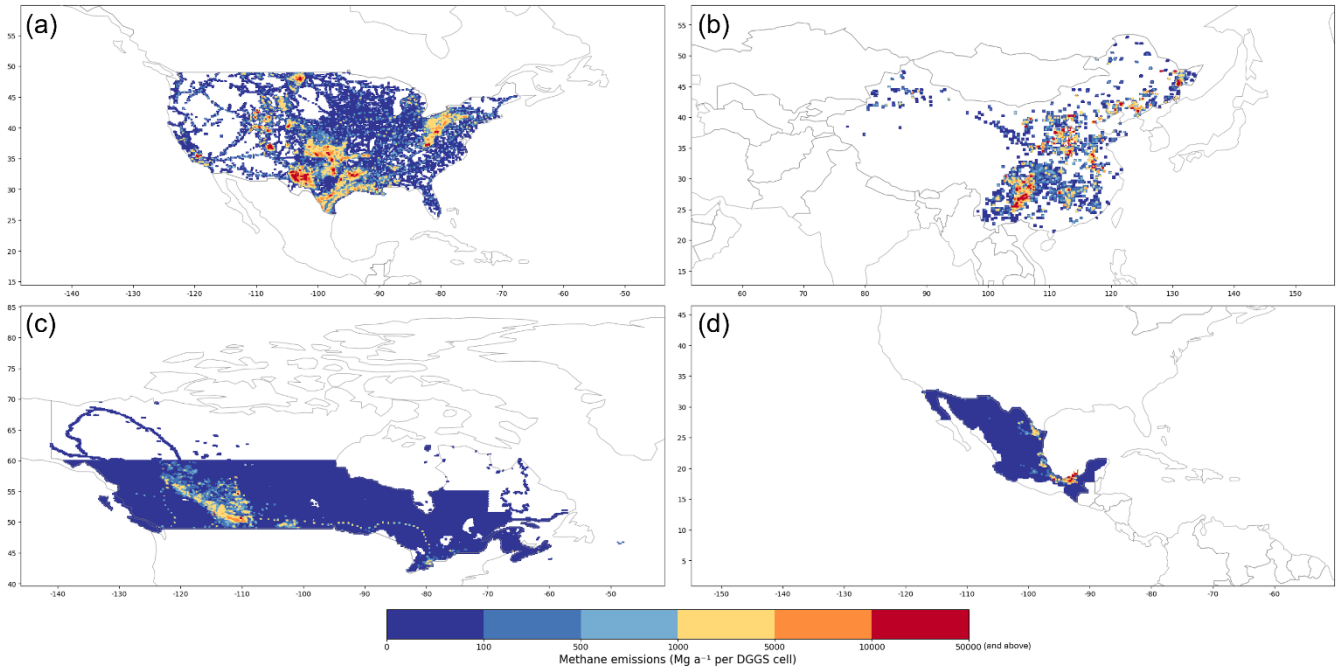

Fig. 5 National-scale energy-sector methane emissions (Mg a^{-1} per DGGS cell) converted to the rHEALPix DGGS at resolution level 6 for (a) continental U.S. Oil and Gas Methane Emissions in 2021 [28], (b) mainland China Coal Mine Methane Emissions in 2011 [30], (c) CMS Datasets on Methane Flux for Oil and Gas Systems in Canada in 2013 [29], and (d) CMS Datasets on Methane Flux for Oil and Gas Systems in Mexico in 2010 [29].

Fig. 6 presents methane emissions from the CAMS-REG v8.1 Emissions Inventory for Europe from 2005 to 2022 [26], shown at DGGS level 7 using a fixed continental color scale. The maps reveal spatially stable emission structures over time, with consistent hotspots associated with major industrial centers. Year-to-year variations are subtle and largely reflect minor adjustments to reported activity data, illustrating the dataset's internal temporal coherence. Fig. 7 and Fig. 8 display the energy sector for the United States (2012-2018) and China (1990-2020), respectively, each with a fixed, within-country color scale to facilitate visual comparison through time [22,24]. The U.S. sequence shows broadly stable spatial patterns with modest interannual variability. In recent years (e.g., 2016-2020), cells in northwest China appear visually less intense than those in eastern and central regions despite the increase in national energy-sector totals shown in Fig. 4. This pattern reflects the absence of fossil-energy consumption emissions reported for these areas in the source inventory and is consistent with the original data. Taken together, these global, continental, national, and temporal examples demonstrate that diverse inventories can be visualized consistently on an equal-area DGGS, supporting transparent side-by-side comparisons.

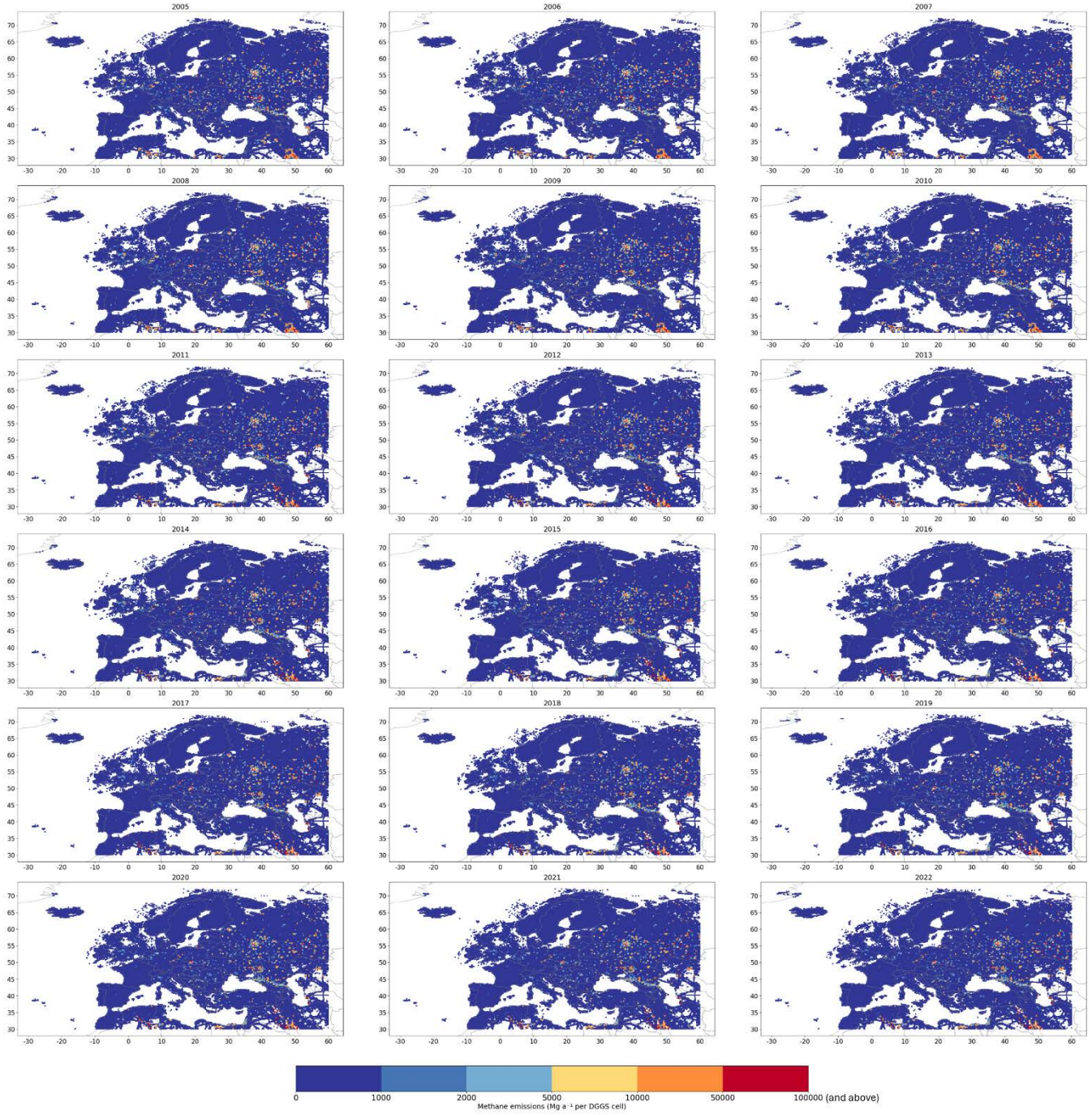

Fig. 6 Energy-sector methane emissions (Mg a^{-1} per DGGS cell) from the CAMS-REG v8.1 Emissions Inventory for Europe [26] for the years 2005-2022, converted to the rHEALPix DGGS at resolution level 7.

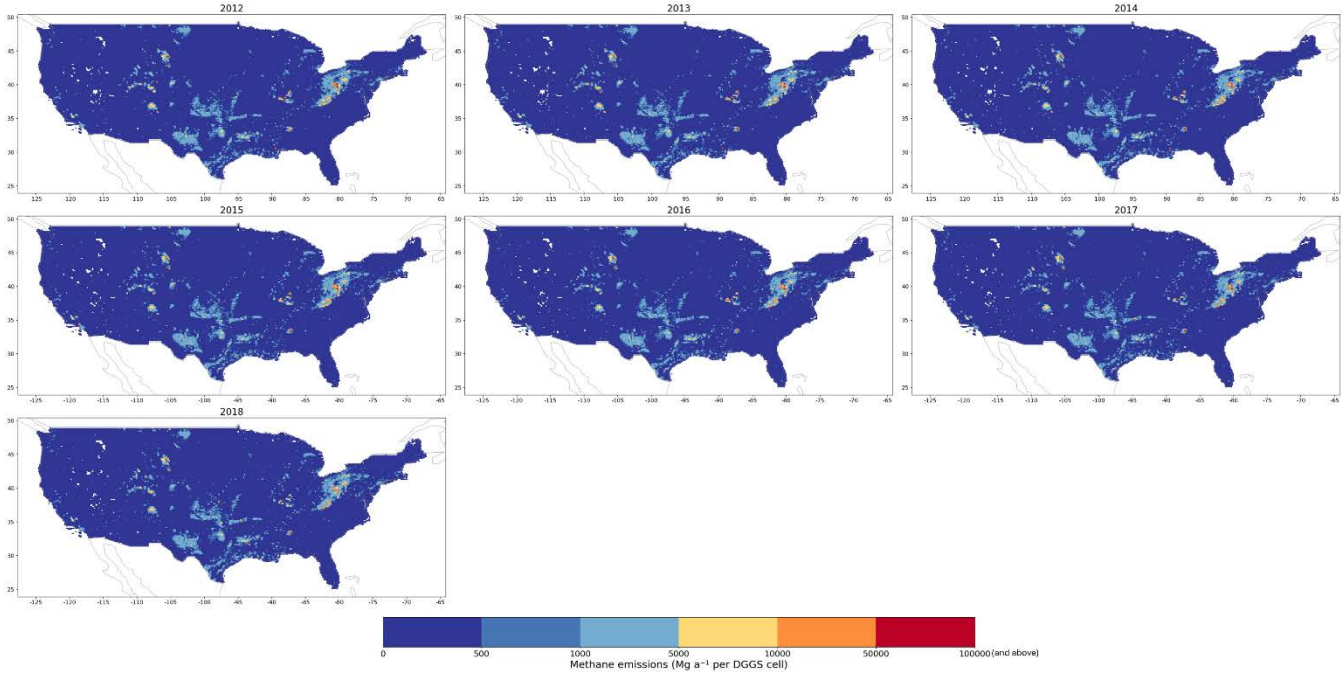

Fig. 7 Energy-sector methane emissions (Mg a^{-1} per DGGS cell) from the continental U.S. Anthropogenic Methane Emissions inventory [22] for the years 2012-2018, converted to the rHEALPix DGGS at resolution level 6.

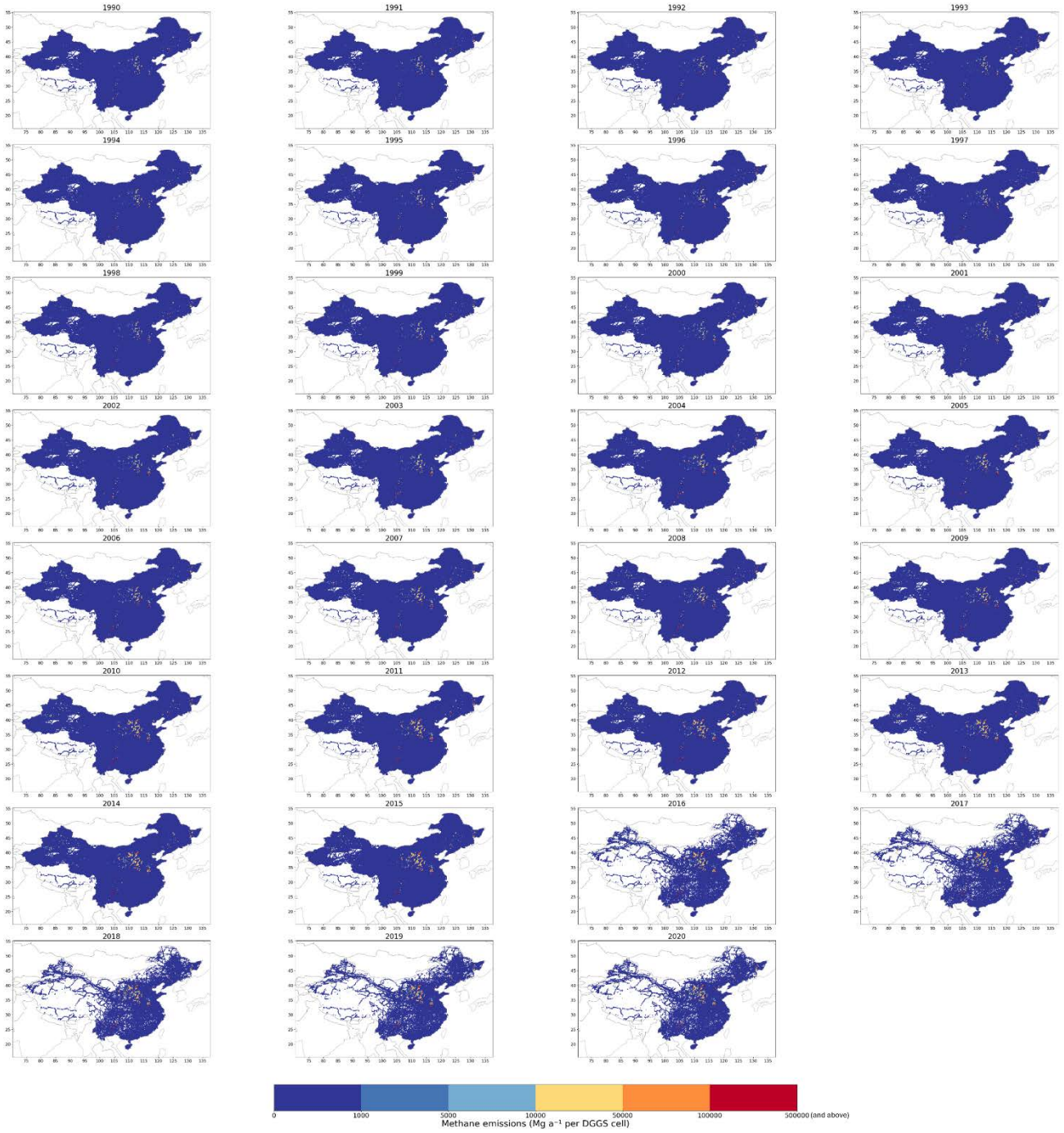

Fig. 8 Energy-sector methane emissions (Mg a^{-1} per DGGS cell) from the mainland China Anthropogenic Methane Emissions inventory [24] for the years 1990-2020, converted to the rHEALPix DGGS at resolution level 6.

Limitations and Use Considerations

This study presents a harmonized collection of global-to-regional methane emission inventories on the rHEALPix DGGS. By standardizing spatial structures, sectoral coding schemes, and reporting units, we resolved the inconsistencies among heterogeneous gridded products. The resulting datasets represent a spatial reformulation of the original gridded products into a DGGS framework. The conversion process is strictly limited to spatial transformation and does not attempt to reassess, correct, or reconcile uncertainties present in the source datasets. All uncertainties associated with the original datasets, including those related to measurement error, sampling representativeness, temporal aggregation, and underlying methodological assumptions, are retained and carried forward. Consequently, datasets generated in this study should be understood as a standardized spatial encoding of the original information rather than an uncertainty-resolved or quality-enhanced product. Any limitations inherent to the source datasets remain unchanged and should be considered in downstream applications.

By representing all sources on rHEALPix DGGS with IPCC 2006 sector codes and values in Mg a^{-1}, users can directly compare emissions between grid cells, countries, years, and data sources and aggregate across sectors, countries, years, and hierarchical grids, without being confounded by differences in projection, cell area, or nomenclature. Because each DGGS cell is fixed in space, temporal trend analysis is straightforward, with temporal changes reflecting changes in emissions rather than shifts in grid definition. In addition, as the cell index follows a hierarchical structure, spatial aggregation can be easily performed by querying cell indices with a common prefix. The dataset and codebase are designed to be extensible. The open converters make it simple to include new inventories as they are released. Once new gridded inventories are released, they can be appended to the unified structure using the same IPCC-2006 crosswalks and unit conversions. The framework also accommodates point-based data, where points are binned to rHEALPix cells in an equal-area, bias-free manner, and incorporated alongside gridded products with full provenance and timestamps. The DGGS index also provides a natural key to integrate future facility information (e.g., wells, compressors, landfills) by linking assets to the cell identifier. In practice, the outputs import cleanly into relational databases, enabling aggregation and filtering by the hierarchical IPCC code system or by ISO country codes for global products. Although this study focuses on methane, the workflow is gas-agnostic, and the same procedures can be extended to other greenhouse gases (e.g., CO_2 and N_2O) and air pollutants (e.g., NO_x, SO_2, and volatile organic compounds).

The standardized fields are suited to a range of applications. They provide priors for inverse atmospheric analyses, where equal-area representation avoids latitudinal biases and IPCC-consistent sectors align with modeling inputs. They provide baseline conditions for simulating large, short-term emission events and for evaluating their detectability against local backgrounds. At finer scales, the products support localized emission estimation and comparison across campaigns, jurisdictions, and sectors, enabling hotspot screening and targeted mitigation planning. More broadly, the uniform scheme and machine-readable structure create a practical foundation for AI-enabled analysis and fast queries across heterogeneous sources. AI has tremendous potential, but it depends on standardized, high-quality data. Emerging spatial standards such as DGGS provide the equal-area and hierarchical semantics needed to unlock that potential. The dataset presented here is AI-ready,

consistent across space, time, units, and sector codes, so it can be ingested directly into modern analytics pipelines for training, inference, and scalable decision support.

Data Availability

The harmonized global to regional gridded methane emission datasets generated in this study are publicly available from the Zenodo repository at https://doi.org/10.5281/zenodo.17362125. The archive contains all converted inventories in rHEALPix DGGS format, including tabular emission data and corresponding GeoParquet geometry files.

Code Availability

The source code to reproduce the datasets is stored in the GitHub repository: https://github.com/GeoSensorWebLab/methane-dggs-converter.

Author Contributions

ML was responsible for data curation, formal analysis, investigation, visualization, and preparation of the original draft. MG contributed to data validation, manuscript review and editing. SL contributed to funding acquisition, supervision, and manuscript review. ML, MG, and SL jointly led the conceptualization of the study.

Competing Interests

The authors declare that they have no conflict of interest.

Acknowledgements

This research was funded by the Rogers Internet of Things Research Chair. We are grateful to the members of the UbiSensing & AI Lab at the University of Calgary for their valuable feedback and collaborative discussions during the development of this study.

References

1 Saunois, M. *et al.* The Global Methane Budget 2000–2017. *Earth System Science Data* **12**, 1561–1623 (2020). https://doi.org/10.5194/essd-12-1561-2020

2 Ishizawa, M. *et al.* Estimation of Canada's methane emissions: inverse modelling analysis using the Environment and Climate Change Canada (ECCC) measurement network. *Atmospheric Chemistry and Physics* **24**, 10013–10038 (2024). https://doi.org/10.5194/acp-24-10013-2024

3 Varon, D. J. *et al.* Continuous weekly monitoring of methane emissions from the Permian Basin by inversion of TROPOMI satellite observations. *Atmospheric Chemistry and Physics* **23**, 7503–7520 (2023). https://doi.org/10.5194/acp-23-7503-2023

4 Maasakkers, J. D. *et al.* Gridded National Inventory of U.S. Methane Emissions. *Environ Sci Technol* **50**, 13123–13133 (2016). https://doi.org/10.1021/acs.est.6b02878

5 Lu, X. *et al.* Methane emissions in the United States, Canada, and Mexico: evaluation of national methane emission inventories and 2010–2017 sectoral trends by inverse analysis of in situ (GLOBALVIEWplus CH4 ObsPack) and satellite (GOSAT) atmospheric observations. *Atmospheric Chemistry and Physics* **22**, 395–418 (2022). https://doi.org/10.5194/acp-22-395-2022

6 Scarpelli, T. R., Jacob, D. J., Moran, M., Reuland, F. & Gordon, D. A gridded inventory of Canada's anthropogenic methane emissions. *Environmental Research Letters* **17**, 014007 (2022). https://doi.org/10.1088/1748-9326/ac40b1

7 Jeong, S., Millstein, D. & Fischer, M. L. Spatially explicit methane emissions from petroleum production and the natural gas system in California. *Environ Sci Technol* **48**, 5982–5990 (2014). https://doi.org/10.1021/es4046692

8 Huang, L., Stokes, S., Chen, Q., Cardoso-Saldaña, F. J. & Allen, D. T. High Spatial and Temporal Resolution Simulations of Methane Column Loadings Due to Routine Emissions and Emission Events in Oil and Gas Regions. *ACS ES&T Air* **1**, 670–677 (2024). https://doi.org/10.1021/acsestair.4c00021

9 Sahr, K., White, D. & Kimerling, A. J. Geodesic discrete global grid systems. *Cartography and Geographic Information Science* **30**, 121–134 (2003). https://doi.org/10.1559/152304003100011090

10 Li, M. & Stefanakis, E. Geospatial operations of discrete global grid systems—a comparison with traditional GIS. *Journal of Geovisualization and Spatial Analysis* **4**, 26 (2020). https://doi.org/10.1007/s41651-020-00066-3

11 Li, M., Tousignant, C., Chaudhuri, C. & Chabbouh, A. Utilizing serverless framework for dynamic visualization and operations in geospatial applications. *International Journal of Digital Earth* **17**, 2392835 (2024). https://doi.org/10.1080/17538947.2024.2392835

12 Rawson, A., Sabeur, Z. & Brito, M. Intelligent geospatial maritime risk analytics using the Discrete Global Grid System. *Big Earth Data* **6**, 294–322 (2021). https://doi.org/10.1080/20964471.2021.1965370

13 Li, M., McGrath, H. & Stefanakis, E. Multi-scale flood mapping under climate change scenarios in hexagonal discrete global grids. *ISPRS International Journal of Geo-Information* **11**, 627 (2022). https://doi.org/10.3390/ijgi11120627

14 Law, R. M. & Ardo, J. Using a discrete global grid system for a scalable, interoperable, and reproducible system of land-use mapping. *Big Earth Data* **9**, 29–46 (2024). https://doi.org/10.1080/20964471.2024.2429847

15 Jendryke, M. & McClure, S. C. Spatial prediction of sparse events using a discrete global grid system; a case study of hate crimes in the USA. *International Journal of Digital Earth* **14**, 789–805 (2021). https://doi.org/10.1080/17538947.2021.1886356

16 Jendryke, M. & McClure, S. C. Mapping crime – Hate crimes and hate groups in the USA: A spatial analysis with gridded data. *Applied Geography* **111**, 102072 (2019). https://doi.org/10.1016/j.apgeog.2019.102072

17 Mechenich, M. F. & Zliobaite, I. Eco-ISEA3H, a machine learning ready spatial database for ecometric and species distribution modeling. *Sci Data* **10**, 77 (2023). https://doi.org/10.1038/s41597-023-01966-x

18 Scarpelli, T. R. *et al.* A global gridded ($0.1° \times 0.1°$) inventory of methane emissions from oil, gas, and coal exploitation based on national reports to the United Nations Framework Convention on Climate Change. *Earth System Science Data* **12**, 563–575 (2020). https://doi.org/10.5194/essd-12-563-2020

19 Scarpelli, T. R. *et al.* Updated Global Fuel Exploitation Inventory (GFEI) for methane emissions from the oil, gas, and coal sectors: evaluation with inversions of atmospheric methane observations. *Atmospheric Chemistry and Physics* **22**, 3235–3249 (2022). https://doi.org/10.5194/acp-22-3235-2022

20 Scarpelli, T. R. *et al.* Using new geospatial data and 2020 fossil fuel methane emissions for the Global Fuel Exploitation Inventory (GFEI) v3. *Earth System Science Data* **17**, 7019–7033 (2025). https://doi.org/10.5194/essd-2024-552

21 Crippa, M. *et al.* GHG emissions of all world countries. Report No. JRC134504, (European Commission, Luxembourg, 2023).

22 Maasakkers, J. D. *et al.* A Gridded Inventory of Annual 2012-2018 U.S. Anthropogenic Methane Emissions. *Environ Sci Technol* **57**, 16276–16288 (2023). https://doi.org/10.1021/acs.est.3c05138

23 Scarpelli, T. R. *et al.* A gridded inventory of anthropogenic methane emissions from Mexico based on Mexico's national inventory of greenhouse gases and compounds. *Environmental Research Letters* **15**, 105015 (2020). https://doi.org/10.1088/1748-9326/abb42b
24 Guo, F., Dai, F., Gong, P. & Zhou, Y. CHN-CH4: A Gridded (0.1°×0.1°) Anthropogenic Methane Emission Inventory of China from 1990 to 2020. *Earth System Science Data* **17**, 4799–4819 (2025). https://doi.org/10.5194/essd-17-4799-2025
25 Hiller, R. V. *et al.* Anthropogenic and natural methane fluxes in Switzerland synthesized within a spatially explicit inventory. *Biogeosciences* **11**, 1941–1959 (2014). https://doi.org/10.5194/bg-11-1941-2014
26 Kuenen, J. *et al.* CAMS-REG-v4: a state-of-the-art high-resolution European emission inventory for air quality modelling. *Earth System Science Data* **14**, 491–515 (2022). https://doi.org/10.5194/essd-14-491-2022
27 Loman, M. L., Murray, L. T., Leibensperger, E. M. & Maasakkers, J. D. A High-Resolution Inventory of Anthropogenic Methane Emissions in New York State. *Environ Sci Technol* **59**, 16933–16946 (2025). https://doi.org/10.1021/acs.est.5c07245
28 Omara, M. *et al.* Constructing a measurement-based spatially explicit inventory of US oil and gas methane emissions (2021). *Earth System Science Data* **16**, 3973–3991 (2024). https://doi.org/10.5194/essd-16-3973-2024
29 Sheng, J.-X. *et al.* A high-resolution (0.1° × 0.1°) inventory of methane emissions from Canadian and Mexican oil and gas systems. *Atmospheric Environment* **158**, 211–215 (2017). https://doi.org/10.1016/j.atmosenv.2017.02.036
30 Sheng, J., Song, S., Zhang, Y., Prinn, R. G. & Janssens-Maenhout, G. Bottom-Up Estimates of Coal Mine Methane Emissions in China: A Gridded Inventory, Emission Factors, and Trends. *Environmental Science & Technology Letters* **6**, 473–478 (2019). https://doi.org/10.1021/acs.estlett.9b00294
31 Sadavarte, P. *et al.* A high-resolution gridded inventory of coal mine methane emissions for India and Australia. *Elementa: Science of the Anthropocene* **10**, 00056 (2022). https://doi.org/10.1525/elementa.2021.00056
32 Gorski, K. M. *et al.* HEALPix — a framework for high resolution discretization, and fast analysis of data distributed on the sphere. *The Astrophysical Journal* **622**, 759–779 (2005). https://doi.org/10.1086/427976
33 Gibb, R. in *IOP Conference Series: Earth and Environmental Science, 9th Symposium of the International Society for Digital Earth (ISDE)* Vol. 34 012012 (IOP Publishing Ltd, Halifax, Canada, 2016).
34 Li, M. E. & Liang, S. H. L. Enabling a Digital Earth for Methane Emissions Management with Equal-Area Discrete Global Grids. *International Journal of Digital Earth* **19**, 2607210 (2026). https://doi.org/10.1080/17538947.2025.2607210
35 St-Louis, J. *DGGAL, the Discrete Global Grid Abstraction Library*, <https://github.com/ecere/dggal> (2025).
36 GADM. *GADM maps and data (version 4.1)*, <https://gadm.org/index.html> (2025).
37 Omara, M. *et al.* Developing a spatially explicit global oil and gas infrastructure database for characterizing methane emission sources at high resolution. *Earth System Science Data* **15**, 3761–3790 (2023). https://doi.org/10.5194/essd-15-3761-2023
38 uraster: Structured Raster to Unstructured Mesh (2026). https://doi.org/10.5281/zenodo.18249075
39 UNFCCC. *Mapping of the categories in the 2006 IPCC Guidelines for National Greenhouse Gas Inventories and those in the common reporting tables (CRT)*, <https://unfccc.int/sites/default/files/resource/Mapping_Categories_CRT-2006IPCCGLs.pdf> (2023).
40 IPCC. 2006 IPCC Guidelines for National Greenhouse Gas Inventories. Report No. 4-88788-032-4, (National Greenhouse Gas Inventories Programme, Japan, 2006).

Supplementary Information for

Harmonized global to regional gridded methane inventories in a discrete global grid framework

Mingke Erin Li[1], Mozhou Gao[2], Steve H.L. Liang[1,2]

[1]Department of Geomatics Engineering, Schulich School of Engineering, University of Calgary, Calgary, Canada
[2]SensorUp Inc., Calgary, Canada

Correspondence to: Mingke Erin Li (mingke.li@ucalgary.ca)

Table of Contents

Source Gridded Inventories

Global Inventory

Emissions Database for Global Atmospheric Research (EDGAR) v8.0 Greenhouse Gas Emissions

The EDGAR is a long-standing global inventory of greenhouse gas and air pollutant emissions developed by the European Commission Joint Research Centre. The latest release, EDGAR v8.0, offers global gridded emissions of CO_2, CH_4, N_2O, and fluorinated gases for the period from 1970 to 2022 at a 0.1° × 0.1° resolution. For methane, EDGAR combines official international activity statistics with IPCC methodological guidelines to compute country-level sectoral totals, which are then downscaled to grid cells using high-resolution spatial proxies [1,2].

Methane emissions in EDGAR v8.0 are reported across the major IPCC sectors, covering energy (power generation, fuel exploitation, and combustion in industry and buildings), agriculture (enteric fermentation, manure management, soils, and crop residue burning), industry (chemical processes and metals production), transport (road, shipping, rail, and aviation), and waste (landfills, wastewater, and incineration). The spatialization of these emissions relies on more than 130 proxy datasets, including the Global Energy Monitor for fossil fuel infrastructure, the Global Human Settlement Layer for population and built-up areas, and satellite observations such as VIIRS nightlights for gas flaring [1,2]. These proxies ensure consistent allocation of national totals to point sources (e.g. coal mines and oil and gas facilities), line sources (e.g. shipping routes and road networks), and area sources e.g. livestock density and crop distribution; [1,2].

Global Fuel Exploitation Inventory (GFEI)

The GFEI is a global gridded dataset of methane emissions from oil, gas, and coal exploitation, provided at 0.1° × 0.1° spatial resolution [3-5]. The inventory is constructed by combining national emissions reported to the UNFCCC with independent estimates for non-reporting countries, supplemented with IPCC Tier 1 methods and energy activity data. National totals are then spatially distributed to grid cells using detailed geospatial information on energy infrastructure, such as oil and gas wells, pipelines, refineries, and coal mines [3-5].

Three major versions of GFEI have been released. Version 1 (2016) provided the first global grid of fossil fuel methane emissions by subsector [5]. Version 2 (2019) expanded temporal coverage to 2010-2019 and incorporated improved national reports, well and pipeline datasets, and coal mine distributions [4]. The latest release, Version 3 (2020), further aligns national emissions with updated UNFCCC submissions and integrates new infrastructure databases, including the Oil and Gas Infrastructure Mapping database and the Global Coal Mine Tracker [3,6]. For coal, mine-level emission factors based on depth and grade are applied to distribute emissions within countries. These improvements result in more spatially accurate emissions patterns, particularly in key emitting regions such as China, Russia, and Central Asia.

Continental inventories

Copernicus Atmosphere Monitoring Service Regional (CAMS-REG) Emissions Inventory for Europe

CAMS-REG is a high-resolution, policy-aligned regional inventory for the United Nations Economic Commission for Europe (UNECE) designed to support air-quality and greenhouse-gas applications [7]. It provides annually gridded emissions at 0.05° × 0.1° on a latitude-longitude grid, delivered as NetCDF or CSV, with complete sectoral detail and ancillary profiles. Methane is included alongside the main air pollutants NO_x, SO_2, CO, NH_3, NMVOC, PM_{10}, and $PM_{2.5}$. Core activity data draw on officially reported national inventories such as UNFCCC for greenhouse gases and European Monitoring and Evaluation Programme or European Economic Area for air pollutants, with gap-filling and consistency checks against Greenhouse gas Air pollution Interactions and Synergies (GAINS), where reporting is incomplete or inconsistent [7,8]. Spatialization is applied uniformly across Europe using sector-specific proxies, including point sources from facility-level registries for power and industry, population and land-use proxies for distributed combustion and agriculture, detailed road-network intensities for transport, and a dedicated Ship Traffic Emission Assessment Model for sea and inland shipping [7]. Semi-natural and natural sources are excluded to maintain alignment with national anthropogenic totals [7].

Multiple operational releases exist. The peer-reviewed baseline (v4.1) documents methods and the 2000-2017 time series [7], and the subsequent releases (v5.1, v6.1, v7.0, and v8.1) extend temporal coverage and incorporate methodological updates (e.g., revised spatial proxies, notably for road transport) while preserving the same gridding and sectoral logic. CAMS-REG v8.1 was used in this study.

National Inventory

U.S. Anthropogenic Methane Emissions

The U.S. Anthropogenic Methane Emissions dataset provides gridded estimates of methane emissions across the contiguous United States for 2012-2018 at 0.1° × 0.1° resolution [9]. It is based on the U.S. Environmental Protection Agency's Greenhouse Gas Inventory, which reports national and state-level emissions by sector to the UNFCCC. These totals are spatially allocated using detailed activity data and infrastructure maps to generate consistent annual emission grids [9]. The dataset covers 26 source categories, including emissions from coal mining, oil and gas systems, landfills, wastewater treatment, and residential combustion. To support finer temporal analysis, monthly scaling factors are provided that reflect seasonal variability across sectors. In addition, an "Express Extension" dataset expands coverage through 2020 with 27 categories, though this extension is not included in the current study.

Canada Anthropogenic Methane Emissions

The Canadian anthropogenic methane inventory provides a high-resolution (0.1° × 0.1°) gridded dataset for 2018, developed by Scarpelli, et al. [10]. It spatially allocates methane emissions from Canada's National Inventory Report submitted to the UNFCCC, integrating facility-level data from Environment and Climate Change Canada's Greenhouse Gas Reporting Program. The inventory disaggregates emissions by major source sectors, including oil and gas, livestock, solid waste, coal, wastewater, and residential combustion, and further resolves the oil and gas sector

by source type (e.g., venting, leakage, flaring, abandoned wells, and oil sands). The dataset leverages an ensemble of Canadian geospatial datasets, such as the CanVec facility and infrastructure maps, provincial activity data (e.g., Alberta and Saskatchewan venting and flaring reports), the Census of Agriculture, and the Biomass Inventory Mapping and Analysis Tool. The dataset identifies 11 national hotspots emitting more than one metric ton h^{-1}, primarily associated with oil sands operations and large municipal landfills [10].

Mexico Anthropogenic Methane Emissions

The Mexican anthropogenic methane inventory provides a high-resolution (0.1° × 0.1°) gridded dataset for 2015 [11]. It spatially disaggregates methane emissions from Mexico's National Inventory of Greenhouse Gases and Compounds, compiled by the Instituto Nacional de Ecología y Cambio Climático (INECC) and reported to the UNFCCC. Major source sectors include livestock (47%), fugitive fuel emissions (20%), solid waste (15%), and wastewater (14%). The oil and gas sector is further resolved by source type, with offshore production alone accounting for about 51% of emissions [11]. The dataset was constructed using a suite of national geospatial databases, including facility-level information from Mexico's Sistema de Información de Hidrocarburos, the national economic unit registry, and sectoral datasets for livestock, waste management, and wastewater treatment [11]. 16 grid cells exceed 20 Gg a^{-1}, highlighting concentrated hotspots of emissions from landfills, oil and gas operations, coal mines, and industrial facilities [11].

China Anthropogenic Methane Emissions

The CHN-CH_4 inventory provides a high-resolution gridded dataset of anthropogenic methane emissions for mainland China covering 1990 to 2020 [12]. It is reported to have a resolution of about 10 km × 10 km and is compiled in GeoTIFF format under the Krasovsky 1940 Albers projection. The dataset covers eight major source sectors including rice cultivation, livestock, biomass and biofuel burning, coal exploitation, oil and natural gas systems, fossil fuel combustion, landfills, and wastewater. The inventory was constructed using a combination of long-term satellite products (e.g., CCD-Rice, WorldPop, impervious surface datasets), national statistical yearbooks (China Agricultural, Energy, and Environmental Statistics), and existing global inventories such as EDGAR v8.0 and Climate TRACE [12]. Provincial emission factors tailored to Chinese conditions were applied where available, supplemented by IPCC 2006 guidelines and the 2019 Refinement. Activity data were downscaled to the grid level using proxies, including gridded GDP, population, and land cover [12].

Switzerland Greenhouse Gas Inventory

The Switzerland Greenhouse Gas Inventory provides a spatially explicit methane dataset at 500 m × 500 m resolution in the national CH1903/LV03 projection [13]. This inventory integrates anthropogenic and natural methane sources into a consistent grid, enabling detailed national-scale assessments. Anthropogenic emissions include livestock, manure management, solid waste, wastewater, fossil fuel combustion, and industrial processes, compiled from Switzerland's National Inventory Report to the UNFCCC [13]. Spatial allocation was performed using a combination of national land-use and population datasets, facility-level information (e.g., waste facilities, wastewater plants, refineries), and sector-

specific models. Emission factors were derived from IPCC 2006 guidelines and adapted to Swiss conditions using measurements and national statistics [13]. In addition to anthropogenic sources, the dataset also accounts for natural methane fluxes from lakes, wetlands, wild animals, and soils, although these were treated separately in the original study [13].

U.S. Oil and Gas Methane Emissions

The U.S. Oil and Gas Methane Emissions dataset provides a spatially explicit, measurement-informed inventory for 2021 at 0.1° × 0.1° resolution [14]. Unlike traditional bottom-up inventories that rely solely on activity data and emission factors, this dataset integrates extensive site-level methane measurements from U.S. oil and gas production facilities with national infrastructure and production databases [14]. Facility-level emission rates were assigned based on observed distributions of methane loss rates across production basins, and spatialized using data from Enverus Prism (well counts and production), the U.S. Environmental Protection Agency Greenhouse Gas Reporting Program, and supplementary infrastructure maps for refineries, compressors, and pipelines [14]. The resulting gridded inventory covers all major onshore production basins and associated infrastructure, providing one of the most detailed and empirically constrained representations of methane emissions from the U.S. oil and gas sector to date. Emissions are provided in kg h^{-1} aggregated to grid cells, with uncertainty bounds derived from repeated Monte Carlo simulations of facility-level emissions distributions [14].

Carbon Monitoring System (CMS) Datasets on Methane Flux for Canadian and Mexican Oil and Gas Systems

The CMS methane datasets for Canada (2013) and Mexico (2010) provide 0.1° × 0.1° gridded estimates of oil and gas methane emissions, developed by Sheng, et al. [15] under NASA's Carbon Monitoring System program. These inventories were designed to serve as improved priors for atmospheric inverse modeling by providing more accurate spatial patterns of emissions. The inventories are built from national bottom-up reports, Canada's estimates from ICF International and Mexico's from the Mexican Petroleum Institute, and employ IPCC Tier 2/3 methods with country-specific emission factors [15]. To generate gridded fields, emissions were spatially allocated using detailed infrastructure and activity datasets, including oil and gas well locations (Drillinginfo), pipeline and compressor station maps, and facility-level processing and refining data. Emissions are resolved by subsector (production, processing, transmission, distribution, and petroleum systems) to capture basin-level differences [15].

China Coal Mine Methane Emissions

The China Coal Mine Methane inventory provides a gridded estimate of methane emissions from coal mining activities in 2011 at 0.25° × 0.25° resolution [16]. It was developed using the most comprehensive publicly available dataset of Chinese coal mines from the State Administration of Coal Mine Safety (SACMS), which reported methane emissions from over 10,000 mines during annual safety evaluations [16]. Methane emissions were derived by combining reported coal mine measurements with province-specific emission factors (distinguishing high- and low-CH_4 content mines) and applying adjustments for methane capture and utilization. Facility names from SACMS were geocoded to obtain mine locations, with additional manual verification for the largest emitters, and emissions were aggregated into the

0.25° grid. Uncertainty estimates were also calculated for each province to support the use of the dataset in atmospheric inversions. The inventory offers a more accurate spatial representation of CMM emissions across China, particularly in key producing provinces such as Shanxi, Sichuan, and Guizhou [16].

India and Australia Coal Mine Methane Emissions

Sadavarte, et al. [17] developed a high-resolution 0.1° × 0.1° gridded inventory of coal mine methane emissions for India and Australia, two of the world's largest coal producers. The dataset provides a bottom-up estimate for 2018, designed to improve the spatial localization of coal mine sources and to reduce uncertainties in regional methane budgets [17]. For India, emissions were estimated using a Tier 2 IPCC methodology combined with country-specific emission factors derived from field measurements at surface and underground mines by the Central Institute of Mining and Fuel Research. Mine-level coal production data and mine type were used to calculate emissions, with mine locations identified using government statistics, the Global Coal Mine Tracker, and remote sensing imagery [17]. For Australia, state-level CMM emissions reported to the UNFCCC (using IPCC Tier 2/3 methods) were spatially disaggregated to individual mines based on production volumes and basin-specific gas content profiles. The study relied on detailed national inventory reporting, coal mine databases, and mine-level production records to allocate emissions [17].

Regional Inventory

Gridded New York State Methane Emissions Inventory

The Gridded New York State Methane Emissions Inventory provides a high-resolution, 100 m × 100 m dataset of anthropogenic methane emissions for New York State in 2020 [18]. Unlike national-scale products with coarser resolution, the Gridded New York State Methane Emissions Inventory was developed to support urban- and regional-scale monitoring, validation, and mitigation planning by providing spatial detail down to the facility and neighborhood level [18]. The dataset was generated by spatially allocating New York State's methane emissions using a combination of state and federal inventories and facility-level activity data [18]. Infrastructure databases and geospatial proxies such as landfill footprints, wastewater treatment plant locations, livestock density maps, and oil and gas well records were used to distribute emissions to grid cells [18]. Emissions are reported in kg m^{-2} s^{-1} and provided in the UTM Zone 18N projection.

Supplementary Tables

Table S1. Annual comparison of total methane emissions before and after rHEALPix DGGS conversion for the EDGAR v8.0 inventory (1970-2022). Absolute and percentage differences indicate numerical consistency between the original and converted datasets.

Year	Total Emissions before Conversion (Mg a^{-1})	Total Emissions after Conversion (Mg a^{-1})[1]	Absolute Difference (%)
1970	244640086.78	244213826.26	0.17
1971	247732604.35	247299624.33	0.17
1972	251141582.60	250596879.25	0.22
1973	257209998.63	256448646.20	0.30
1974	258780821.22	257649461.33	0.44
1975	261732970.80	261371339.20	0.14
1976	264815820.54	262660256.07	0.81
1977	267388824.64	265241225.18	0.80
1978	268902333.41	266872066.37	0.76
1979	273054091.18	271015928.06	0.75
1980	271727781.20	269895199.34	0.67
1981	267441113.09	265813969.01	0.61
1982	268814631.12	267266432.90	0.58
1983	269842292.96	268218224.04	0.60
1984	274197304.94	272418285.54	0.65
1985	276765722.42	274967554.94	0.65
1986	280775209.25	278866262.70	0.68
1987	282865307.53	280850464.00	0.71
1988	288551045.42	286382741.88	0.75
1989	294594755.00	292231573.46	0.80
1990	294670363.61	292304166.09	0.80
1991	292968211.45	290503290.04	0.84
1992	292886406.81	290256912.94	0.90
1993	292203877.32	289372040.12	0.97
1994	294169891.34	290995373.00	1.08
1995	297984592.85	294759736.40	1.08
1996	301064302.34	297373847.51	1.23
1997	300686383.82	296714873.70	1.32
1998	297177998.66	293358964.24	1.29
1999	298385843.85	294518029.68	1.30
2000	302327759.24	298224666.14	1.36
2001	302487603.92	298422449.95	1.34
2002	302346726.18	298385088.20	1.31
2003	311439703.93	307102439.37	1.39
2004	318463238.45	313947797.12	1.42
2005	324700709.14	320041921.48	1.43
2006	331220211.09	326440274.01	1.44
2007	334514630.69	329787324.72	1.41
2008	340159909.09	335277428.99	1.44
2009	339233313.42	334415043.01	1.42
2010	346214967.57	341225619.61	1.44
2011	354488226.01	349429427.58	1.43
2012	358160346.24	352940577.94	1.46
2013	359709447.49	354389546.12	1.48
2014	362263780.25	356913264.16	1.48
2015	363644850.47	358324810.56	1.46

2016	365234492.59	359818427.63	1.48
2017	370275878.81	364560747.93	1.54
2018	376578581.08	371089508.55	1.46
2019	379476326.78	374020307.16	1.44
2020	375833285.38	370911676.80	1.31
2021	381627191.72	376635778.65	1.31
2022	388175521.87	382859913.52	1.37

[1] Reported values from the original datasets were standardized to units of Mg a^{-1} for consistency and comparison.

Table S2. Annual comparison of total methane emissions before and after rHEALPix DGGS conversion for the CAMS-REG V8.1 inventory (2005-2022). Absolute and percentage differences indicate numerical consistency between the original and converted datasets.

Year	Total Emissions before Conversion (Mg a^{-1})	Total Emissions after Conversion (Mg a^{-1})[1]	Absolute Difference (%)
2005	58948955	58948948	1.18E-05
2006	58759945	58759955	1.60E-05
2007	58048420	58048420	1.48E-06
2008	57758134	57758134	1.23E-06
2009	56940168	56940168	8.69E-07
2010	56851049	56851037	2.15E-05
2011	57330395	57330396	1.48E-06
2012	57306957	57306970	2.28E-05
2013	56765400	56765402	3.90E-06
2014	56602100	56602110	1.79E-05
2015	57048963	57048966	4.66E-06
2016	58798610	58798609	2.09E-06
2017	59282927	59282924	4.06E-06
2018	59767758	59767761	4.93E-06
2019	59434747	59434755	1.23E-05
2020	59307306	59307311	9.47E-06
2021	59154966	59154977	1.77E-05
2022	59180701	59180695	1.04E-05

Table S3. Annual comparison of total methane emissions before and after rHEALPix DGGS conversion for the U.S. Anthropogenic Methane Emissions inventory (2012-2018). Results confirm conservation of total emissions across all years within the DGGS framework.

Year	Total Emissions before Conversion (Mg a^{-1})	Total Emissions after Conversion (Mg a^{-1})[1]	Absolute Difference (%)
2012	25626259.09	25692238.00	0.26
2013	25514454.95	25590870.68	0.30
2014	25386293.08	25473164.61	0.34
2015	25370927.66	25503835.72	0.52
2016	24730454.55	24843235.43	0.46
2017	25030265.57	25167637.08	0.55
2018	25225964.39	25368622.74	0.57

[1] Reported values from the original datasets were standardized to units of Mg a^{-1} for consistency and comparison.

Table S4. Annual comparison of total methane emissions before and after rHEALPix DGGS conversion for the China Anthropogenic Methane Emissions inventory (1990-2020). Differences represent rounding-level variation associated with spatial aggregation to the DGGS grid.

Year	Total Emissions before Conversion (Mg a^{-1})	Total Emissions after Conversion (Mg a^{-1})[1]	Absolute Difference (%)
1990	24676397.28	24676397.28	1.27E-10
1991	25087692.19	25087692.19	1.26E-10
1992	25761668.71	25761668.71	1.01E-10
1993	26490005.86	26490005.86	8.97E-11
1994	28101775.11	28101775.11	7.72E-11
1995	30087615.26	30087615.26	8.69E-11
1996	28900433.71	28900433.71	8.82E-11
1997	29580793.48	29580793.48	8.39E-11
1998	30038425.47	30038425.47	7.76E-11
1999	29976905.63	29976905.63	9.03E-11
2000	28417742.36	28417742.36	7.99E-11
2001	30554758.41	30554758.41	6.19E-11
2002	31664920.01	31664920.01	5.92E-11
2003	34026330.09	34026330.09	4.73E-11
2004	37769568.92	37769568.92	3.60E-11
2005	39750395.13	39750395.12	3.81E-11
2006	41277802.64	41277802.64	4.25E-11
2007	39612828.16	39612828.16	3.49E-11
2008	40407658.73	40407658.73	3.43E-11
2009	41941928.14	41941928.14	3.29E-11
2010	45339490.63	45339490.62	1.88E-11
2011	47419795.38	47419795.37	2.02E-11
2012	47751732.33	47751732.33	1.55E-11
2013	47450418.55	47450418.55	2.10E-11
2014	47813379.08	47813379.08	2.52E-11
2015	48196809.56	48196809.56	2.09E-11
2016	45697687.92	45697687.92	2.35E-10
2017	46202960.34	46202960.34	2.32E-10
2018	46677240.84	46677240.84	2.41E-10
2019	46533957.48	46533957.48	2.30E-10
2020	46431934.67	46431934.67	2.32E-10

[1] Reported values from the original datasets were standardized to units of Mg a^{-1} for consistency and comparison.

References

1 Crippa, M. *et al.* GHG emissions of all world countries. Report No. JRC134504, (European Commission, Luxembourg, 2023).

2 Crippa, M. *et al.* Insights into the spatial distribution of global, national, and subnational greenhouse gas emissions in the Emissions Database for Global Atmospheric Research (EDGAR v8.0). *Earth System Science Data* **16**, 2811–2830 (2024). https://doi.org/10.5194/essd-16-2811-2024

3 Scarpelli, T. R. *et al.* Using new geospatial data and 2020 fossil fuel methane emissions for the Global Fuel Exploitation Inventory (GFEI) v3. *Earth System Science Data* **17**, 7019–7033 (2025). https://doi.org/10.5194/essd-2024-552

4 Scarpelli, T. R. *et al.* Updated Global Fuel Exploitation Inventory (GFEI) for methane emissions from the oil, gas, and coal sectors: evaluation with inversions of atmospheric methane observations. *Atmospheric Chemistry and Physics* **22**, 3235–3249 (2022). https://doi.org/10.5194/acp-22-3235-2022

5 Scarpelli, T. R. *et al.* A global gridded (0.1° × 0.1°) inventory of methane emissions from oil, gas, and coal exploitation based on national reports to the United Nations Framework Convention on Climate Change. *Earth System Science Data* **12**, 563–575 (2020). https://doi.org/10.5194/essd-12-563-2020

6 Omara, M. *et al.* Developing a spatially explicit global oil and gas infrastructure database for characterizing methane emission sources at high resolution. *Earth System Science Data* **15**, 3761–3790 (2023). https://doi.org/10.5194/essd-15-3761-2023

7 Kuenen, J. *et al.* CAMS-REG-v4: a state-of-the-art high-resolution European emission inventory for air quality modelling. *Earth System Science Data* **14**, 491–515 (2022). https://doi.org/10.5194/essd-14-491-2022

8 Höglund-Isaksson, L., Gómez-Sanabria, A., Klimont, Z., Rafaj, P. & Schöpp, W. Technical potentials and costs for reducing global anthropogenic methane emissions in the 2050 timeframe –results from the GAINS model. *Environmental Research Communications* **2** (2020). https://doi.org/10.1088/2515-7620/ab7457

9 Maasakkers, J. D. *et al.* A Gridded Inventory of Annual 2012-2018 U.S. Anthropogenic Methane Emissions. *Environ Sci Technol* **57**, 16276–16288 (2023). https://doi.org/10.1021/acs.est.3c05138

10 Scarpelli, T. R., Jacob, D. J., Moran, M., Reuland, F. & Gordon, D. A gridded inventory of Canada's anthropogenic methane emissions. *Environmental Research Letters* **17**, 014007 (2022). https://doi.org/10.1088/1748-9326/ac40b1

11 Scarpelli, T. R. *et al.* A gridded inventory of anthropogenic methane emissions from Mexico based on Mexico's national inventory of greenhouse gases and compounds. *Environmental Research Letters* **15**, 105015 (2020). https://doi.org/10.1088/1748-9326/abb42b

12 Guo, F., Dai, F., Gong, P. & Zhou, Y. CHN-CH4: A Gridded (0.1°×0.1°) Anthropogenic Methane Emission Inventory of China from 1990 to 2020. *Earth System Science Data* **17**, 4799–4819 (2025). https://doi.org/10.5194/essd-17-4799-2025

13 Hiller, R. V. *et al.* Anthropogenic and natural methane fluxes in Switzerland synthesized within a spatially explicit inventory. *Biogeosciences* **11**, 1941–1959 (2014). https://doi.org/10.5194/bg-11-1941-2014

14 Omara, M. *et al.* Constructing a measurement-based spatially explicit inventory of US oil and gas methane emissions (2021). *Earth System Science Data* **16**, 3973–3991 (2024). https://doi.org/10.5194/essd-16-3973-2024

15 Sheng, J.-X. *et al.* A high-resolution (0.1° × 0.1°) inventory of methane emissions from Canadian and Mexican oil and gas systems. *Atmospheric Environment* **158**, 211–215 (2017). https://doi.org/10.1016/j.atmosenv.2017.02.036

16 Sheng, J., Song, S., Zhang, Y., Prinn, R. G. & Janssens-Maenhout, G. Bottom-Up Estimates of Coal Mine Methane Emissions in China: A Gridded Inventory, Emission Factors, and Trends. *Environmental Science & Technology Letters* **6**, 473–478 (2019). https://doi.org/10.1021/acs.estlett.9b00294

17 Sadavarte, P. *et al.* A high-resolution gridded inventory of coal mine methane emissions for India and Australia. *Elementa: Science of the Anthropocene* **10**, 00056 (2022). https://doi.org/10.1525/elementa.2021.00056

18 Loman, M. L., Murray, L. T., Leibensperger, E. M. & Maasakkers, J. D. A High-Resolution Inventory of Anthropogenic Methane Emissions in New York State. *Environ Sci Technol* **59**, 16933–16946 (2025). https://doi.org/10.1021/acs.est.5c07245